Journal of Materials Chemistry C

Accepted Manuscript

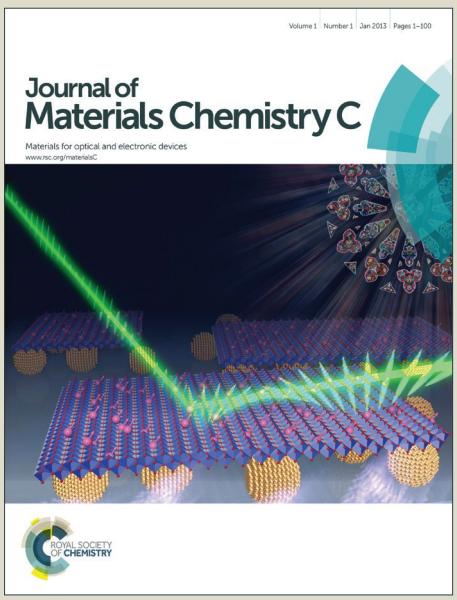

ROYAL SOCIETY OF CHEMISTRY

www.rsc.org/materialsC

Monitoring *in vitro* Neural Stem Cells Differentiation based on Surfaces–Enhanced Raman Spectroscopy using Gold Nanostars array

Waleed Amed El-Said[1,4], Seung U. Kim[2] and Jeong-Woo Choi[1, 3*]

[1]*Interdisciplinary program of Integrated Biotechnology, Sogang University, 35 Baekbeom-Ro, Mapo-Gu, Seoul 121-742, Republic of Korea*

[2]*Department of Medicine, Faculty of Medicine, University of British Columbia, Vancouver, British Columbia, Canada*

[3]*Department of Chemical and Biomolecular Engineering, Sogang University, 35 Baekbeom-Ro, Mapo-Gu, Seoul 121-742, Republic of Korea*

[4]*Department of Chemistry, Faculty of Science, Assiut University, Assiut, 71516, Egypt*

*Correspondence: Prof. Jeong–Woo Choi

Department of Chemical and Biomolecular Engineering

Sogang University, Seoul, Republic of Korea

Tel. +82–2–705–8480; Fax: +82–2–3273–0331.

E-mail: jwchoi@sogang.ac.kr

Abstract: The development of neurochips for non-invasive monitoring neural stem cells stimulation is highly desirable issue, and can enable the efficient optimization of tissue development protocols. Traditional methods including cell staining and sorting, have long been used, but these techniques are time consuming and may damage cells. Here, we have developed a cell-based chip to monitor the *in-vitro* stepwise differentiation process of embryonic stem cells (ESCs), the one-step differentiation of adult human neural stem cells (HB1.F3), and the electrochemical stimulation of rat pheochromocytoma PC12 cells. Results showed that each cell line exhibited a different behavior during differentiation. The DNA contents changed in an irregular manner during the differentiation of the HB1.F3 cells, while the percentage of proteins increased. In addition, the results revealed that the electrochemical stimulation of PC12 cells induced changes in the synthesis of DNA and proteins. The differentiation of ESCs showed a decrease in some peaks corresponding to the DNA content and an increase in the percentage of protein, in addition to the irregular behavior of some peaks related to both nucleic acids and proteins. The increase in the protein percentage could indicate local variations in protein structure and a maturation shift. These results demonstrate that the SERS technique allows for more rapid biological sample analysis without time-consuming staining, enabling researchers to monitor engineered tissues and optimize culture conditions in a near real time manner.

Keywords: Embryonic neural stem cells; Surface-enhanced Raman spectroscopy; Adult neural stem cells; Differentiation, Electrochemical stimulation.

Introduction

Embryonic stem cells have the ability to differentiate into one of more than 200 cell types, such as neurons, cardiomyocytes, hepatocytes, islet cells, skeletal muscle cells, and endothelial cells.[1] Stem cell therapy could change the treatment of intractable human diseases such as Parkinson's disease, ischemic heart diseases, and diabetes.[2] Neural stem cells (NSCs) have considerable therapeutic potential for the treatment of neurological disorders. The differentiation of NSCs is an important process during the development of the central nervous system.[3] Therefore, monitoring the differentiation of NSCs is of importance in different fields, such as regenerative medicine, transplantable tissue, and as an alternative source of donor tissue neural precursors. Further applications include the repair of pathological processes and the repair of neurodegenerative processes, including Parkinson's and Alzheimer's diseases.[1,4] In addition, understanding the mechanisms of *in-vitro* stem cell differentiation will allow the development of rational approaches to systematically manipulate cell fates. Common methods reported for monitoring the differentiation of neural cells include the reverse transcription polymerase chain reaction (RT-PCR), immunohistochemistry, immunocytochemistry, colorimetric, or sorting techniques.[5] However, these techniques have a number of disadvantages, such as being labor-intensive multistep processes, being endpoint assays that do not offer the

mechanism details, being time consuming, or being destructive methods requiring biomarkers or labels thereby, limiting potential application. The development of an efficient high-throughput, rapid, simple, sensitive, nondestructive and label-free technique for *in-vitro* monitoring of the differentiation of NSCs on a single cell level is therefore needed. This would have an impact on biomedicine as well as on the development of effective stem cell sensors.[6]

Cell-based chips hold great promise for cell-based detection methods, through the use of optical or electrochemical detection systems. Electrochemical cell-based chips allow for easy monitoring and analysis of the cell signals of living cells arising from redox reactions;[7] utilizing several electrochemical techniques such as cyclic voltammetry (CV), differential pulse voltammetry, electric cell-substance impedance sensing (ECIS), scanning electrochemical microscopy (SECM), electrochemical impedance spectroscopy (EIS), and the oxygen electrode.[8] In our previous studies, the voltammetric behaviors of different cancer cells was determined using modified electrodes. These studies reported on the effect of anti-cancer drugs on a cell chip using CV and potential stripping analysis methods.[9] However, the electrochemical behavior of the living cells represented only the cell viability based on electron transfer between the cell and the electrode surface, and the

mechanism of the stem cell differentiation could not be monitored using these electrochemical methods.

Cell-based chips for optical detection have the distinct advantage of being able to visualize changes in cell status.[10] While, white light imaging (phase contrast or differential interference contrast) can reveal the approximate level of *in-situ* differentiation, it is a qualitative technique. Fourier transform infrared (FT–IR) spectroscopy can be used for monitoring the single cell differentiation of fixed or dried stem cells, but is not suitable for monitoring the differentiation of living cells. Although Raman spectroscopy has demonstrated the ability to monitor the differentiation of living NSC, it is too slow to characterize a sufficient number of individual cells to be a reliable clinical technique. Nonetheless, Raman spectroscopy could be used extensively in biomedical research.[11]

The enhancement factors in surface-enhanced Raman spectroscopy (SERS) can be as high as 10^9-10^{15}, which allows this technique to be sensitive enough to detect single molecules.[12] In addition, SERS has 2 to 3 times the sensitivity as compared to fluorescence.[13] As such, the increased sensitivity of Raman scattering has generated tremendous interest in the nanomaterial, spectroscopy, and analytical chemistry communities.[14] SERS offers an exciting opportunity to overcome the critical

disadvantages of the conventional Raman spectroscopy, allowing for relatively lower laser intensity, longer wavelengths, and rapid signal acquisition times. Consequently, near infrared (NIR)-SERS is becoming a useful tool for biological applications[15] with high selectivity and sensitivity, which could extend Raman utility to a wide variety of interfacial systems previously inaccessible to conventional Raman spectroscopy. In addition, the SERS technique gives effective molecule specific information regarding immobilized molecules on the metal surface, *in-situ,* and in aqueous solutions. At present, many researchers continue to demonstrate the great potential of SERS applications in the fields of biochemistry, biophysics, and molecular biology. Average SERS enhanced spectra is one of two strategies to acquire the SERS signals,[16] which are obtained from an ensemble of colloidal particles and aggregates giving a relatively low signal especially before aggregation. Several studies have reported on the use of colloidal metallic (gold (Au) or silver (Ag)) nanoparticles (NPs) or nanorods to perform SERS on living cells and various important biological species such as DNA and protein.[17] Au NPs of different diameters were used as SERS-active agents for monitoring chemical changes during the differentiation of embryonic stem cells (ESCs).[18] However, the non-homogeneity of the NP aggregates caused a dramatic change in the enhancement of Raman signal from one point to another on the cell surface. During the NP preparation some surfactants such as

CTAB (cetyltrimethylammonium bromide) or PVP (polyvinylpyrrolidone) were used.[19] The existence of these species on the metal NP surface results in fewer active sites, and the SERS signal generated by these species could severely interfere with the SERS signals of the target molecules. Samanta et al. (2014) reported on the fabrication of specific targeting SERS nanotags based on the modification of Au NPs with three active Raman reporters and antibodies for the identification of differentiated ESCs.[20] The antibody-conjugated metal NPs could overcome the non-homogeneity limitations of non-targeting NPs. However, the presence of antibodies was reported to cause unwanted SERS signals that were barely distinguishable from the Raman signals originating from target molecules inside the cell.[21] In addition, nuclear-targeted Au NPs have been used as intracellular probes to monitor the differentiation of ESCs using SERS.[22] This was a challenge, due to the existence of several cellular barriers limiting the delivery of SERS–active colloidal NPs to the cell nucleus.[23] Moreover, Au NPs–targeting of the cell nucleus has been reported to influence cellular function, causing DNA damage, cell death, and apoptosis.[24]

The development of SERS-active surfaces has been based on the existence of particular hot spots (Ag or Au nanostructures) on modified substrates, which permits the detection of a few molecules with fluctuating spectral characteristics.[25] However, the

fabrication of SERS-active substrates has been found to create a number of problems, including poor signal enhancement, uniformity, and reproducibility. In previous work conducted by our group, we developed different SERS-active surfaces to monitor anticancer effects as well as to analyze intracellular states.[26, 27] An advanced method for the fabrication of SERS-active surfaces is still required for more effective enhancement of Raman signals.

The present work represents the development and application of an Au nanostructures modified ITO substrate as a SERS-active surface, cell culture system, and working electrode, as shown in Scheme 1. These provide a quantitative, label-free, biocompatible, and noninvasive optical spectroscopy technique for monitoring the *in-vitro* stepwise differentiation process of ESCs, the one-step differentiation of adult human neural stem cells (HB1.F3), and the electrochemical stimulation of rat pheochromocytoma PC12 cells. Thus, the approach described in this paper plays a vital role in identifying the cell types in biomedical stem cell research, overcoming the limitations of the SERS-NPs-based approach. Moreover, this technique is a promising noninvasive tool to monitor the changes in the chemical composition of NSCs during their differentiation, and has potential applications in high throughput analysis, drug screening, and induced pluripotent stem cell generation.

Experimental Section

Materials. Hydrogen tetrachloroaurate (III) trihydrate ($HAuCl_4 \cdot 3H_2O$, 99.9+ %), and phosphate buffered saline (PBS) (pH 7.4, 10 mM) solution were purchased from Sigma-Aldrich (St. Louis, MO, USA). Neurite growth factor (NGF) was obtained from Millipore. Polyethylene glycol-200 (PEG) (MW = 200) was obtained from Yakuri Pure Chemicals Co. Ltd. (Osaka, Japan). All other chemicals used in this study were obtained commercially as reagent grade chemicals. All aqueous solutions were prepared using deionized water (DIW) deionized with a Millipore Milli-Q water purifier operating at a resistance of 18 MΩ cm.

Cell culture. Rat neural PC12 cells, ES cells and HB1.F3 were cultured in DMEM supplemented with 10% heat inactivated fetal bovine serum (FBS; Gibco, Carlsbad, CA, USA) and 1% antibiotics (Gibco). The cells were maintained under standard cell culture conditions at 37 °C in an atmosphere of 5 % CO_2. The medium was changed every two days. The number of cells was determined by the trypan blue assay with a hemacytometer.

Electrochemical measurements. All electrochemical experiments were performed using a potentiostat (CHI-660, CH Instruments, USA) controlled by general-purpose

electrochemical system software. A homemade three-electrode system consisting of cell/Au nanostars/ITO as the working electrode, a platinum wire as the counter electrode and Ag/AgCl as the reference electrode was set up. Measurements were carried out to study the electrical properties of living cells under normal laboratory conditions. PBS (10 mM, pH 7.4) was used as an electrolyte at a scan rate of 50 mV/s.

Raman spectroscopy. The biochemical composition of the control PC12, HB1.F3 and ES cells, as well as the effect of one step differentiation on PC12 cells and HB1.F3 cells or of stepwise differentiation of ES cells were investigated based on the SERS technique using Raman NTEGRA spectra (NT-MDT, Russia) equipped with an inverted optical microscope and a liquid nitrogen-cooled CCD detector. The maximum scan-range, XYZ, was 100 μm × 100 μm × 6 μm, and the resolution of the spectrometer in the XY plane was 200 nm and along the Z axis was 500 nm. Raman spectra were recorded using an NIR laser emitting light at a wavelength of 785 nm with an irradiation laser power of 3 mW on the sample plane. The medium was removed and the cells were washed three times with PBS, which was used during the SERS measurements for eliminating the effect of the medium on SERS signals. Ten scans of 5 s from 600-1750 cm^{-1} were recorded and the mean result was used. A blank spectrum was acquired prior to each step, which allowed the absorbance to be subsequently measured.

Fabrication of gold nanostars array modified ITO substrate. Au nanostars arrays were electrochemically deposited onto ITO substrates (20 mm × 10 mm) using different concentrations of a $HAuCl_4$ aqueous solution containing 20 µL/mL of PEG-200 as a surfactant, according our previously reported method.[27] The, ITO-coated glass substrates were typically cleaned by sequential sonication in 1% Triton X-100 solution, DIW, and ethanol for 15 min, followed by sonication in basic piranha solution (1:1:5, H_2O_2:NH_3:H_2O) for 30 min at 80 ºC. Finally, the substrates were rinsed with DIW and dried under a N_2 stream to obtain a clean ITO surface. Au nanostar arrays were electrochemically deposited onto the ITO substrates by using different concentrations of $HAuCl_4$ (0.3, 0.5 and 0.7 mM) under a constant potential of -1.3 V (vs. Ag/AgCl), and the deposition temperature was controlled and maintained at 25 ºC in an electric-heated thermostatic water bath. To remove any trace surfactants adsorbed on the Au nanostars modified ITO surface, the substrates were rinsed in DIW then boiled for 5 min with isopropyl alcohol under a N_2 stream. The active area for electrochemical deposition of the Au nanostars was 10 x 10 mm, and their surface morphologies were analyzed using a scanning electron microscope (SEM) (ISI DS-130C, Akashi Co., Tokyo, Japan), as shown in Figure 1.

SERS Monitoring of the Differentiation of ES Cells. To monitor the differentiation of the ES cells, approximately 2 × 10^4 mouse ES cells were assembled on an Au nanostars/ITO substrate surface (20 mm x 10 mm) for 28 days. The cells were examined at 14 time points, beginning with the Raman spectrum for adhered cells (day 0), and then every 48 hrs after the cell had adhered to the surface of the substrate. SERS mapping was been conducted for each cell, and the Raman spectrum from 20 points was extracted. The mean Raman spectrum of each observed time point during mouse ES cells differentiation is offset and overlaid in Figure 6.

In-vitro PC12 Electrochemical Stimulation. Electrochemical stimulation of the neurite outgrowth of PC12 was developed based on a previously reported method.[28] Typically, PC12 cells were assembled onto an Au nanostars/ITO substrate at a density of 2 x 10^4 cells/cm^2, then incubated for 24 h to permit attachment and spreading. The PC12 cells were subjected to a steady potential of 100 mV for 2 h. For electrical stimulation, the Au nanostars/ITO served as the anode, an Au wire placed at the opposite end (along the length) of the well served as the cathode and an Ag wire served as a quasi-reference electrode. The cells were maintained in a CO_2 incubator for the duration of the electrical stimulation. After the electrical stimulation, the cells were incubated for an additional 24

h (for a total of 48 h from the start of the experiment). Using SEM, the lengths of the neuritis of the cells under stimulation were compared with controls to estimate the extent of differentiation.

Results and Discussion

Development of Gold nanostars/ITO substrate

Au nanostars are biocompatible nanoconstructs that represent a promising nanoplatform for various biomedical applications, such as SERS,[29] photodynamic therapy,[30] photothermal therapy,[31] photoacoustic imaging,[32] and biosensing.[33] In this study, Au nanostar modified ITO substrates were developed by reduction of $HAuCl_4$, using electrochemical deposition in the presence of PEG-200 as a structure directing agent. Figures 1 (a-c) show SEM images of the Au nanostars/ITO substrates prepared using different concentrations of $HAuCl_4$, revealing the formation of Au 3D-nanostructures 40 nm in diameter. The nanostar morphology consists of multiple perpendicular branches within the same plane, but at slightly different angles. In addition, the density of Au nanostructures is increased by increasing the concentration of $HAuCl_4$, as shown in Figures 1 (a-c). Figure 1-d shows the UV-Vis spectra of three Au nanostars/ITO substrates ranging from 350–800 nm. The absorption spectra of the Au

nanostars/ITO substrates demonstrate that Au nanostars have two broad surface plasmon absorption peaks; one at around 553 nm, resulting from transverse electronic oscillation, and the other in the NIR region (704 nm), due to the longitudinal oscillation of conduction band electrons. These two plasmon bands result from the hybridization of the plasmon from branches that act as "hot spots" due to the "lightning rod" effect.[34] Because of the heterogeneous branch morphology, nanostar ensembles probably enable a wider range of LSPR modes, which explains the broadening of the extinction spectra. In addition, the plasmon peak intensity increased with increasing density of the Au nanostars, as the intensity depends on the branch number/length.[34]

SERS Monitoring of the Electrical Stimulation of PC12 Cells

The rat pheochromocytoma PC12 cell line has been reportedly used as a model system for neuronal differentiation by electrical stimulation or treatment with nerve growth factor.[35] In this study, we used the PC12 cell line as a model system for neuronal differentiation by electrical stimulation, by applying a steady potential of 100 mV for 2 h to the cells. The SEM technique was used to confirm the differentiation of PC12. Figure 2b shows SEM image of control PC12 and also the show SEM images of PC12 after cell stimulation were showed in Figures 2c & 2d, which demonstrate the changes in

morphology and the apparent enlargement of neurons extending from the cell body after cell stimulation. The Raman spectrum of the control PC12 is shown in Figure 2a, which shows Raman peaks at 775 cm^{-1} (Trp, U, C and T), 1001 cm^{-1} (Phe), 1092 cm^{-1} (PO_2^-), 1205 cm^{-1} (Phe and Trp), 1230 cm^{-1} (amide III and T), 857 cm^{-1} (Tyr), 1490 cm^{-1} (G and A) and 1620 cm^{-1} (C=C Trp and Tyr str.).[36] Moreover, the peak at 1270 cm^{-1} corresponds to the presence of amide III and catecholamines such as dopamine (DA). The Raman peak at 1557 cm^{-1} was assigned to C=C str. of a phenyl group. These data corresponds to earlier published cell spectra.[37] On the other hand, the Raman spectrum of the differentiated PC12 cells exhibit changes in several Raman peaks. These changes included a decrease in the Raman peak intensities at 1001 cm^{-1} (Phe), and 1170 cm^{-1} (pro, C−C/C−N str.). Conversely, the intensities of the Raman peaks at 775 cm^{-1} and 1097 cm^{-1} (PO_2^- of nucleic acids) increased after cell differentiation. Moreover, new Raman peaks appeared at 857 cm^{-1} (Tyr), 875 cm^{-1} (lipids, C−C−N^+ str. and carbohydrate C−O−C ring), 1450 cm^{-1} (carbohydrate δCH_2), and 1490 cm^{-1} (nucleic acids, G and A). On the other hand, the Raman peak at 1470 cm^{-1} (pro. def CH) was disappeared after the differentiation of PC12. These results illustrate the ability of the SERS-active surface to monitor the differentiation of PC12 cells. In addition, the electrical stimulation of the PC12 cells induces changes in DNA and protein synthesis.

SERS Monitoring the Differentiation of HB1F3 Cells

The SERS technique was also applied to monitor the differentiation of HB1.F3 cells as shown in Figure 3. Figure 3 exhibit a typical Raman peaks including characteristic peaks corresponding to nucleotide and sugar-phosphate backbone vibrations such as peak at 690 cm^{-1} (DNA, G), 796 cm^{-1} (PO_2^- in DNA, U, C and T), 1310 cm^{-1} (A) and 838 cm^{-1} (PO_2^- in RNA). The protein contents were dominated by Raman peaks corresponding to amide II (1540 cm^{-1}), 913 (Ring str. CC), 955 (str. CC α-helix), 1120 (CN str.), 1155 (CC/CN str.), 1214 cm^{-1} (amide III β-sheet) and 1284 cm^{-1} (amide III) vibrations. Amino acids could be identified by peaks corresponding mainly to phenyl groups, such as Phe (1001 cm^{-1}), Trp (730 and 755 cm^{-1}), Trp vibrations (1540 cm^{-1}), Tyr vibrations (838 cm^{-1}) and 1617 cm^{-1} (C=C Trp, Try). The Raman peaks of lipids were present at 730 cm^{-1}, 1452 cm^{-1} (CN str), 1388 cm^{-1} (CH def), and 1097 cm^{-1} (hydrocarbon chains vib.). Carbohydrates were detected by the identification of Raman peaks for sugars, especially the COC vibrations of sugar rings (1047 cm^{-1} and 1284 cm^{-1}), and at 1440 cm^{-1} (dCH_2), 1400 cm^{-1} (dCOO), and 1120 cm^{-1} (CO str. carbohydrate). In comparison to the undifferentiated HB1.F3 cells, the Raman spectrum for differentiated HB1.F3 cells (Figure 3) demonstrated a decrease in Raman peaks intensities at 755 cm^{-1} (A and Trp),

838 cm^{-1} (Tyr and PO_2^- in RNA/DNA), 913 cm^{-1} (pro, Ring str. CC), 955 cm^{-1} (pro, str. CC α-helix), 1155 cm^{-1} (pro, CC/CN str.), 1440 cm^{-1} (carbohydrate, dCH_2) and 1540 cm^{-1} (Trp and amide II). Raman peak intensities at 690 cm^{-1} (DNA, G) and 1120 cm^{-1} (CO str. carbohydrate) increased after cell differentiation. These results indicate that some contents of DNA (A and PO_2^- in DNA) decrease during the differentiation of stem cells; while, G/DNA increases. On the other hand, the percentage of most proteins contents (Trp, Tyr, pro, Ring str. CC, str. CC α-helix, str. pro. CC/CN) decreases, indicating local variations in protein structure.

Cyclic Voltammetry Monitoring the Differentiation of HB1F3 Cells

In addition, a CV technique was used to monitor the differentiation of HB1.F3 cells. The cyclic voltammetric behavior of undifferentiated HB1.F3 cells over the potential range of +0.6 to -0.2 V exhibited a quasi-reversible redox process with a cathodic peak at +0.13 V and an anodic peak at +0.25 V. The voltammetric behavior of the cells was recorded for 25 cycles. The results demonstrated that with an increase in the number of CV cycles no change in the potential peaks could be observed, but there was a slight decrease in peak current (Figure 4a). In addition, the differentiated HB1.F3 cells exhibited quasi-reversible redox behavior with a cathodic peak at +0.13 V and an anodic

peak at +0.21 V. The voltammetric behavior of the cells showed a decrease in the peak current with an increase in number of cycles (Figure 4b). It of note that the differentiate HB1.F3 cells showed a higher current peak than the undifferentiated cells. The peak-peak separation of undifferentiated HB1.F3 cells (120 mV) is more than that of the differentiated HB1.F3 cells (80 mV), indicating higher reversibility of the differentiated HB1.F3 cells than of the undifferentiated HB1.F3 cells (Figure 4c). The high reversibility of differentiated HB1.F3 cells is related to the nature of neurons, in which the membrane potential very rapidly undergoes a large change (hyperpolarization or depolarization). This is in contrast to non-excitable cells, in which the membrane potential is held at a relatively stable value (resting potential).

SERS Analyze of Undifferentiated Living ES Cells

The differentiation process of neural ES cells is characterized by its differentiation over a long period. Thus, the differentiation process was monitored over time as a stepwise process. Figure 5 shows optical images of ES cells during differentiation over 28 days, which illustrate the changes in the morphology and appearance of neurons that extend from the cell body. The length of the neurons increased with increased differentiation time.

Figure 6a shows the Raman spectrum of undifferentiated ESCs, exhibiting characteristic Raman peaks corresponding to nucleotide and sugar-phosphate backbone vibrations. These include the Raman peaks at 1097 cm^{-1} (PO_2^-), 796 cm^{-1} (PO_2^- bonds in DNA, U, C and T) and 824 cm^{-1} (PO_2^- bonds in RNA). Different protein contents were dominated by Raman peaks corresponding to amide II (1570 cm^{-1}), amide III ß-sheet (1214 cm^{-1}) and amide III (1284 cm^{-1}). Moreover, amino acids could be identified by peaks corresponding mainly to phenyl groups, such as Phe 1001 cm^{-1} (C-C ring breathing: Phe/protein), Trp (724 and 762 cm^{-1}), and Tyr vib. (838 and 1570 cm^{-1}). The Raman peaks of lipids present at 724 cm^{-1}, 1452 cm^{-1} (CN str.), 1388 cm^{-1} (CH def.), and 1097 cm^{-1} correspond to vibrations of the hydrocarbon chains. Carbohydrates were also detected by identification of the Raman peaks of sugars, especially the COC vibrations of sugar rings (1051, 1097 and 1284 cm^{-1}), and CH def. at 1388 cm^{-1}. The peak assignments of the spectrum are presented in Table 1.

SERS Real Time Monitoring the Differentiation of ES Cells

Ami et al., (2008) and Zelig et al., (2010) have reported that nucleic acids in undifferentiated cells were decreased in compared to differentiated cells[4]; while, Schulze and his group (2010) have shown high contents of nucleic acids in

undifferentiated cells[38]. On the other hand, some studies have demonstrated that the protein composition[39,40] have been increased compared to differentiated cells have been described[4]. However, such increases have also been also associated with the differentiation process[38].

The SERS technique was used as a real time tool to monitor the differentiation on ES cells. The SERS results of ES cells during differentiation (Figure 6b) demonstrated that the intensities of some Raman peaks changed. New peaks appeared while others disappeared during the differentiation of ES cells. The change in the Raman spectrum at several Raman shifts represents varying amounts of biochemical components, including nuclear material, DNA/RNA bases, the DNA backbone, amino acids, proteins, and lipids, as indicated by changes in the intensity of the peaks at 650 (Tyr), 738 (Trp), 828 (Trp and DNA/RNA PO_2), 850 (Trp), 1001 (Phe), 1160 (proteins C-N/C-C str.), 1220 (DNA/RNA bases T and A), 1340 (bases of DNA/RNA G and A), 1580 (proteins (CH) and lipids, bases of DNA/RNA G and A), and at 1617 cm^{-1} (prot, C=C Trp and Tyr).

The behavior of the Raman intensity changes at each peak was monitored. Peaks at 650 cm^{-1} (Tyr) and 1160 cm^{-1} (pro, CN/CC star.) appeared after the cells had adhered to the substrate for two weeks, and the intensity increased with culture time, as shown in Figures 7a & 7b. Figures 7c and 7d demonstrate that the intensities of the Raman peaks at

738 cm^{-1} (Trp) and 1617 cm^{-1} (pro, (C=C Trp and Tyr)) increased with culture time, which indicates that the percentage of these protein components increased as culture time increased. However, these peaks disappeared after two weeks. Similarly, Figure 8a shows that the intensity of the Raman peak at 828 cm^{-1} (Trp and to DNA/RNA PO_2) increased with culture time for two weeks and then disappeared. The Raman peak intensities at 850 cm^{-1} (Trp), 1220 cm^{-1} (bases of DNA/RNA (T and A) and proteins (amid III)), and 1340 cm^{-1} (bases of DNA/RNA G and A) changed irregularly with culture time, as shown in Figures 8b-d. In addition, the Raman peak intensity at 1001 cm^{-1} (Phe) decreased with culture time (Figure 9a). In contrast, Figure 9b demonstrates that the intensity of the Raman peak at 1580 cm^{-1} (bases of DNA/RNA (G and A)) increased with culture time.

Remarkably, the SERS spectra of the differentiated ESCs demonstrated a significant increase in Raman intensities corresponding to some protein components, such as amino acids, Trp, Tyr, and CN/CC (650, 738 and 1617 cm^{-1}) , which increased. On the other hand, the percentage of Phe (1001 cm^{-1}) decreased during the differentiation process. The percentage of the bases of DNA/RNA (G and A) (1580 cm^{-1}) increased with an increase in the differentiation time. In contrast, it was observed that the intensities of the Raman peaks of proteins and DNA were changed in an irregular manner.

Furthermore, Figures 9c & 9d show that the Raman intensities of nucleic acids

(DNA/RNA composites) at 1580 cm^{-1} were divided by protein-related bands, such as 1001 cm^{-1} (Phe) and 1160 cm^{-1} (CN/CC star.). These results indicate that the Raman peaks for the protein/nucleic acid intensity increased, while the peaks for the proteins components decreased.

The percentage of some protein components in the differentiated ES cells increased, while others decreased, as compared to the undifferentiated cells. This was also observed in the percentage of DNA/RNA components as DNA is the original template for protein synthesis. Thus, a change in the DNA may affect synthesis of the protein. Although previous studies have shown an increase in nucleic acids and proteins in differentiated cells as compared to undifferentiated cells,[38] others have shown opposite results.[39] Our results demonstrated an increase in some nucleic acids and proteins, a decrease in some components, and irregular trends in other components during the differentiation process, which is consistent with previous studies.[38, 39]

To verify our results, the change in the total protein content during ESC differentiation was evaluated based on a colorimetric method using a Diamond GPT kit following the manufacturer's instructions. The culture medium was removed, the adhered cells were washed three times with ice-cold PBS buffer, and the PBS was drained off. 100 μl/10^7 cells in chilled RIPA buffer were then added, the adherent cells scraped off, and the cell

suspension kept for 1 hr. Finally, the cell lysate was collected by centrifuging the suspension at 12000 rpm for 20 min at 4 °C. The total protein concentration of the lysate was determined based on a colorimetric test, in which a standard solution was used. The intensity of the specimen was measured against the reagent blank at 546 nm wavelength after 5 min. Figure 10 shows the change in the total protein content as a function of differentiation time, demonstrating that the total amount of protein increased with increasing differentiation time, which is in agreement with the SERS results.

These findings indicate that there is a change in the percentage of total Raman-active biomolecular components during the differentiation of mouse ES cells.

Conclusions

In summary, these results demonstrate that the Raman technique can be used for real time monitoring of the differentiation of different neural cells (PC12 cells, embryonic stem cells and adult stem cells). Each cell line has a different behavior during differentiation. The differentiation of neural ES cells could be analyzed with time, as it is a stepwise process, which is a challenge in the tissue engineering filed. These results also demonstrate that the DNA content seems to change irregularly during the differentiation of stem cells. The percentage of most proteins components increased, while that of some

proteins components decreased. The increase in the amount of proteins reflects local variations in protein structure and a maturational shift. The results also indicate that the electrostimulation of PC12 cells induces changes in the synthesis of DNA and proteins. The differentiation of ES cells showed irregular changes in DNA content and an increase in protein percentage, in addition to the irregular behavior of some peaks related to both nucleic acids and proteins. Furthermore, the differentiated HB1.F3 cells showed higher reversibility more than the undifferentiated HB1.F3 cells. Therefore, the SERS analysis technique allows for more rapid sample analysis without time-consuming staining.

Acknowledgment

This work was supported by the Leading Foreign Research Institute Recruitment Program through the National Research Foundation of Korea (NRF) funded by the Ministry of Science, ICT & Future Planning (MSIP) (2013K1A4A3055268) and by the National Research Foundation of Korea (NRF) grant funded by the Korea government (MSIP) (2014R1A2A1A10051725).

Table 1. Peak assignments of control ES cell SERS spectrum

Raman shift cm^{-1}	Assignment			
	Proteins	Lipids	Nucleic Acids	carbohydrates
1611	C=C Try, Trp			
1570	Amide II, Trp , Phe, Tyr		G, A	
1498			G, A	
1422			A, G	
1388		CH def		CH def
1323	CH_3CH_2 twist		A, G	
1284	amide III			C-O str.
1214	Amide III βsheetTryp, Phy str.		T, A	
1097		Chain C-C str.	PO_2^- str.	C-O-C glycos.
1051				C-O str.
1001	Sym. Ring br Phe			
960	proteins: v(CC)			
918	Pro.: ring v(CC)			
838	Ring br. Tyr		O-P-O asym. str.	
796			O-P-O str. DNA, U,C,T ring br	
762	Ring breath Trp			
724	Ring br. Trp	C-N head group	A	

Figure Captions

Scheme 1. Schematic diagram for fabrication of neural stem cell-based chip and its applications as cell culture system for SERS/electrochemical monitoring of the stem cell differentiation process.

Figure 1. SEM image of an Au nanostars modified ITO substrate fabricated using aqueous solution of a $HAuCl_4$ of different concentrations **(a)** 0.3 mM, **(b)** 0.5 mM and **(c)** 0.7 mM containing 20 µL/mL of PEG-200 under a constant potential of -1.3 V (vs. Ag/AgCl), and the deposition temperature was maintained at 25 °C. **(d)** UV-vis spectra of the three Au nanostars/ITO substrates. Scale bar 100 nm.

Figure 2. Electrical stimulation of PC12: (a) Raman spectrum for (1) undifferentiated and (2) differentiated PC12 cells within range of 600 cm^{-1} to 1750 cm^{-1}, **(b)** SEM image of undifferentiated PC12 cell, **(c and d)** SEM images of differentiated PC12 cell.

Figure 3. Raman spectra for (1) undifferentiated HB1.F3 cells and (2) differentiated HB1.F3 cells within range of 600 cm^{-1} to 1750 cm^{-1}.

Figure 4. CV monitoring of the differentiation of HB1.F3 cells **(a)** CV for undifferentiated HB1.F3 cells for 25 cycles, **(b)** CV for differentiated HB1.F3 cells for 25 cycles and **(c)** CV for differentiated and undifferentiated HB1.F3 cells. The cell number was 2.1×10^4 cell/ml. Data represent the mean ± standard deviation of three different experiments. PBS (10 mM, pH 7.4) was used as an electrolyte at a scan rate of 50 mV/s.

Figure 5. Optical images of control ES cells (0 day) **(a)** and after 2 **(b)**, 4 **(c)**, 6 **(d)**, 8 **(e)**, 10 **(f)**, 12 **(g)**, 14 **(h)**, 16 **(i)**, 18 **(j)**, 20 **(k)**, 22 **(l)**, 24 **(m)**, 26 **(n)** and 28 **(o)** days of differentiation process.

Figure 6. SERS spectrum for **(a)** undifferentiated ES Cells and **(b)** Real time monitoring of the differentiated ES cells over 28 days within range of 600 cm^{-1} to 1750 cm^{-1}.

Figure 7. Changes in the intensities of some Raman peaks that characterize the protein contents with culture time at different Raman shifts, **(a)** 650 cm^{-1} (Tyr), **(b)** 1160 cm^{-1} (CN/CC star.), **(c)** 738 cm^{-1} (Trp), and **(d)** 1617 cm^{-1} (C=C Trp and Tyr). Data represents the mean ± standard deviation of ten different points.

Figure 8. Changes in the intensities of some Raman peaks that characterize the nucleic acids percentages with culture time at different Raman shift values: **(a)** 828 cm^{-1} (Trp and to DNA/RNA PO_2), **(b)** 850 cm^{-1} (Trp), **(c)** 1220 cm^{-1} (bases of DNA/RNA (T and A) and proteins (amid III)), and **(d)** 1340 cm^{-1} (bases of DNA/RNA G and A). Data represents the mean ± standard deviation of ten different points.

Figure 9. Changes in the intensities of some characteristic Raman peaks with culture time at different Raman shifts: **(a)** 1001 cm^{-1} (Phe) and **(b)** 1580 cm^{-1} (bases of DNA/RNA (G and A)). Raman intensities of nucleic acids (DNA/RNA composites) divided by protein-related bands, **(c)** 1580 cm^{-1}/1001 cm^{-1} (Phe) and **(d)** 1580 cm^{-1}/1160 cm^{-1} (CN/CC star.). Data represents the mean ± standard deviation of ten different points.

Figure 10. The total protein content changes as a function of differentiation time over 28 days.

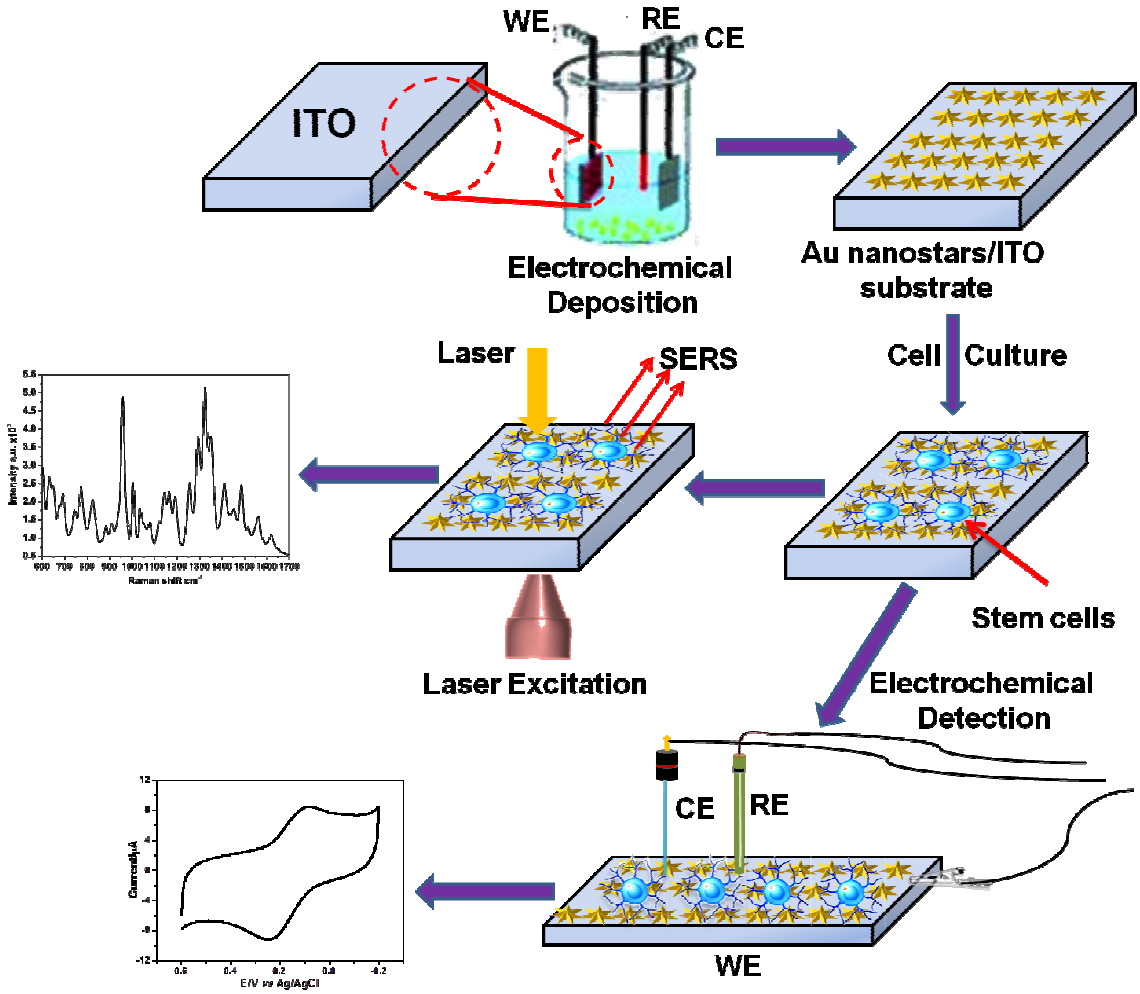

Scheme 1

References

1. B. Coleman, J. B. Fallon, L. N. Pettingill, M. G. de-Silva, R. K. Shepherd, *Experimental Cell Research*, 2007, **2**, 232; K. Takahashi, K. Tanabe, M. Ohnuki, M. Narita, T. Ichisaka, K. Tomoda, S. Yamanaka, *Cell*, 2007, **5**, 861.

2. O. Lindvall, *Pharmacological Research*, 2003, **47** (4) 279.

3. J. Briscoe, B. G. Novitch, *Philos Trans R Soc Lond B Biol Sci*, 2008, **363**, 57.

4. D. Ami, T. Neri, A. Natalello, P. Mereghetti, S.M. Doglia, M. Zanoni, M. Zuccotti, S. Garagna, C.A. Redi, *Biochimica et Biophysica Acta (BBA) - Molecular Cell Research*, 1783 (2008) 98; U. Zelig, Z. Dror, S. Iskovich, A. Zwielly, M. Ben-Harush, I. Nathan, S. Mordechai, J. Kapelushnik, *J. Biomed. Opt.* 2010, **15**, 037008.

5. R. M. Lemoli, F. Bertolini, R. Cancedda, M. De Luca, A. Del Santo, G. Ferrari, S. Ferrari, G. Martino, F. Mavilio, S. Tura, *Haematologica*, 2005, **90**, 360; Y.-S. Hwang, Y. Kang, A. Mantalaris, *Biotechnology and Bioprocess Engineering*, 2007, **12**, 15.

6. J. K. Pijanka, D. Kumar, T. Dale, I. Yousef, G. Parkes, V. Untereiner, Y. Yang, P. Dumas, D. Collins, M. Manfait, G. D. Sockalingum, N. R. Forsyth, J. Sule-Suso, *Analyst*, 2010, **135**, 3126.

7. T.-H. Kim, W. A. El-Said, J.H. An, J.-W. Choi, Nanomedicine: Nanotechnology, Biology and Medicine, 2013, 9 (3), 336; W. A. El-Said, C.-H. Yea, H.H. Kim, J.-W. Choi,

Current Applied Physics, 2009, 9, e76–e80; T.-H. Kim, W. A. El-Said, J.-W. Choi, Biosensors and Bioelectronics, 2012, 32, 266; W. A. El-Said, C.-H. Yea, J.-W. Choi, Il-K. Kwon, Thin Solid Films, 2009, 518, 661; W. A. El-Said, T.-H. Kim, H.C. Kim, J.-W. Choi, Nanotechnology, 2010, 21, 455501 (7pp).

8. A. J. Bard, X. Li, W. Zhan, *Biosensors and Bioelectronics*, 2006, **4**, 461; H. Lu, M. Gratzl, *Analytical Chemistry*, 1999, **14**, 2821; H. F. Cui, J. S. Ye, Y. Chen, S. C. Chong, F. S. Sheu, *Analytical Chemistry*, 2006, **18**, 6347; R. J. Fasching, S.-J. Bai, T. Fabian, F. B. Prinz, *Microelectronic Engineering*, 2006, **4–9**, 1638; T. Kaya, Y. S. Torisawa, D. Oyamatsu, M. Nishizawa, T. Matsue, *Biosensors and Bioelectronics*, 2003, **11**, 1379; S. Kasai, H. Shiku, Y. Torisawa, K. Nagamine, T. Yasukawa, T. Watanabe, T. Matsue, *Analytica Chimica Acta*, 2006, **1**, 55; S. Kasai, H. Shiku, Y. Torisawa, K. Nagamine, T. Yasukawa, T. Watanabe, T. Matsue, *Analytica Chimica Acta*, 2006, **1**, 55; P. Wolf, A. Rothermel, A. G. Beck-Sickinger, A. A. Robitzki, *Biosensors and Bioelectronics*, 2008, **2**, 253.

9. W. A. El-Said, C.H. Yea, H.H. Kim, B.K. Oh, J.-W. Choi, *Biosensors and Bioelectronics*, 2009, **5**, 1259.

10. X. Michalet, F. F. Pinaud, L. A. Bentolila, J. M. Tsay, S. Doose, J. J. Li, G. Sundaresan, A. M. Wu, S. S. Gambhir, S. Weiss, *Science*, 2005, **5709**, 538; R. P. Singh,

B.K. Oh, K. K. Koo, J. Y. Jyoung, S. Jeong, J.W. Choi, *Biochip Journal*, 2008, **4**, 223; L. Zhu, W. Wu, M. Q. Zhu, J. J. Han, J. K. Hurst, A. D. Li, *J. Am. Chem. Soc.*, 2007, **12**, 3524.

11. A. Downes, R. Mouras, A. Elfick, *J Biomed Biotechnol*, 2010, **2010**, 101864.

12. W. E. Doering, and S. M. Nie, *J. Phys. Chem. B.* 2002, **106** (2), 311; S. Nie, S. R. Emory, *Science*, 1997, **275** (5303), 1102.

13. K. Flauds, R. P. Barbagallo, J. T. Keer, W. E. Smith, D. Graham, *Analyst*, 2004, **129**, 567; Y. C. Cao, R. Jin, C. A. Mirkin, *Science*, 2002, **297**, 1536.

14. M. Moskovits, *J. Raman Spectroscopy*, 2005, **36** (6-7), 485; K. Kneipp, H. Kneipp, I. Itzkan, R. R. Dasari, M. S. Feld, *J. Phys. Cond. Matter.* 2002, **14** (18), R597; W. A. El-Said, J.-W. Choi, *Biotechnology and Bioprocess Engineering*, 2014, **19** (6), 1069.

15. M. Volkan, D. L. Stokes, T. Vo-Dinh, *Appl. Spectrosc.* 2000, **54**, 1842.

16. R. Aroca, Surface-Enhanced Vibrational Spectroscopy; John Wiley & Sons, U.K. (2006).

17. K. Kneipp, A. S. Haka, H. Kneipp, K. Badizadegan, N. Yoshizawa, C. Boone, K. E. Shafer-Peltier, J. T. Motz, R. R. Dasari, M. S. Feld, *Appl. Spectrosc.* 2002, **56**, 150; H. W. Tang, X. B. Yang, J. Kirkham, D. A. Smith, *Appl. Spectrosc.* 2008, **62**, 1060; X. Huang, I. H. El-Sayed, W. Qian, M. A. El-Sayed, *Nano Lett.* 2007, **7**, 1591; H. Morjani, J. F. Riou, I.

Nabiev, F. Lavelle, M. Manfait, *Cancer Res.* 1993, **53**, 4784; M. Manfait, H. Morjani, I. Nabiev, *J. Cell. Pharmaco.* 1992, **3**, 120.

18. B. Moody, C. M. Haslauer, E. Kirk, A. Kannan, E. G. Loboa, G. S. McCarty, *Appl. Spectrosc.* 2010, **64**, 1227–1233; R. R. Sathuluri, H. Yoshikawa, E. Shimizu, M. Saito, E. Tamiya, *PLoS ONE*, 2011, **6**, e22802.

19. S. Ayyappan, R. S. Gopalan, G. N. Subbanna, C. N. R. Rao, *J. Mater. Res.* 1997, **12**, 398; C. J. Johnson, E. Dujardin, S. A. Davis, C. J. Murphy, S. Mann, *J. Mater. Chem.* 2002, **12**, 1765.

20. A. Samanta1, R. K. Das, S. J. Park, K. K. Maiti, Y. T. Chang, *Am. J. Nucl. Med. Mol. Imaging*, 2014, **4(2)**, 114-124.

21. M.-D. Li, Y. Cui, M.-X. Gao, J. Luo, B. Ren, Z.-Q. Tian, *Anal. Chem.* 2008, **80**, 5118.

22. A. Huefner, W.-L. Kuan, R. A. Barker, S. Mahajan, *Nano Lett.* 2013, **13**, 2463−2470

23. A. G. Tkachenko, H. Xie, D. Coleman, W. Glomm, J. Ryan, M. F. Anderson, S. Franzen, D. L. Feldheim, *JACS*, 2003, **125**, 4700.

24. Kang B, Mackey MA, El-Sayed MA , J. Am. Chem. Soc. 2010, 132, 1517–1519.

25. E. C. Le Ru, , E. Blackie, M. Meyer, P. G. Etchegoin, *J. Phys. Chem. C*, 2007, **111**, 13794; P. G. Etchegoin, M. Meyer, E. Blackie, E. C. Le Ru, *Anal. Chem.* 2007, **79**, 8411.

26. W. A. El-Said, H.-Y. Cho, C.-H. Yea, J.-W. Choi, *Advanced Materials*, 2014, **26** (6),

910; W. A. El-Said, T.-H. Kim, H.C. Kim, J.-W. Choi, *PLoS ONE*, 2011, 6(2): e15836; W. A. El-Said, T.-H. Kim, Y.-H. Chung, J.-W. Choi, *Biomaterials*, 2015, **40**, 80.

27. W. A. El-Said, T.-H. Kim, H. Kim, J.-W. Choi, *Biosensors and Bioelectronics*, 2010, **26**, 1486.

28. C. E. Schmidt, V. R. Shastri, J. P. Vacanti, R. Langer, *Proceedings of the National Academy of Sciences*, 1997, **94**, 8948.

29. Rodriguez-Lorenzo L, Alvarez-Puebla RA, Pastoriza-Santos I, Mazzucco S, Stephan O, Kociak M, Liz-Marzan LM, Garcia de Abajo FJ. J Am Chem Soc. 2009; 131:4616; Barbosa S, Agrawal A, Rodriguez-Lorenzo L, Pastoriza-Santos I, Alvarez-Puebla RA, Kornowski A, Weller H, Liz-Marzan LM. Langmuir. 2010; 26:14943; Lu W, Singh AK, Khan SA, Senapati D, Yu H, Ray PC. J Am Chem Soc. 2010; 132:18103; Su Q, Ma X, Dong J, Jiang C, Qian W. ACS Appl Mater Interfaces. 2011; 3:1873; Schutz M, Steinigeweg D, Salehi M, Kompe K, Schlucker S. Chem Comm. 2011; 47:4216.

30. Fales AM, Yuan (co-first author) H, Vo-Dinh T. Langmuir. 2011; 27:12186.

31. Van de Broek B, Devoogdt N, D'Hollander A, Gijs HL, Jans K, Lagae L, Muyldermans S, Maes G, Borghs G. ACS Nano. 2011; 5:4319; Yuan H, Khoury CG, Wilson CM, Grant GA, Bennett AJ, Vo-Dinh T. Nanomedicine: NBM.

201210.1016/j.nano.2012.02.005; Yuan H, Fales AM, Vo-Dinh T. J Am Chem Soc. 2012; 134:11358.

32. Kim C, Song HM, Cai X, Yao J, Wei A, Wang LV. J Mater Chem. 2011; 2 1:2841.

33. Dondapati SK, Sau TK, Hrelescu C, Klar TA, Stefani FD, Feldmann J. ACS Nano. 2010; 4:6318.

34. Yuan H, Khoury CG, Hwang H, Wilson CM, Grant GA, Vo-Dinh T. Nanotec hnology. 2012; 23:075102.

35. D. R. Kaplan, R. M. Stephens, *J Neurobiol*, 1994, **25**, 1404; E. Bieberich, A. Guiseppi-Elie, *Biosensors and Bioelectronics*, 2004, **19**, 923.

36. I. Notingher, S. Verrier, S. Haque, J. M. Polak, L. L. Hench, *Biopolymers*, 2003, **72**, 230.

37. R. J. Dijkstra, W. J. J. M. Scheenen, N. Dam, E. W. Roubos, J. J. ter Meulen, *J. Neurosci. Methods*, 2007, **159**, 43.

38. H. G. Schulze, S. O. Konorov, N. J. Caron, J. M. Piret, M. W. Blades, R. F. B. Turner, *Anal. Chem*. 2010, **82**, 5020; W. Tanthanuch, K. Thumanu, C. Lorthongpanich, R. Parnpai, P. Heraud. *J. Mol. Struct.* 2010, **967**, 189; S. O. Konorov, H. G. Schulze, C. G. Atkins, J. M. Piret, S. A. Aparicio, R. F. B. Turner, M. W. Blades, *Anal. Chem.* 2011, **83**,

6254; A. Huefner, W.-L. Kuan, R. A. Barker, S. Mahajan, *Nano Lett.* 2013, **13**, 2463.

39. P. Heraud, E. S. Ng, S. Caine, Q. C. Yu, C. Hirst, R. Mayberry, A. Bruce, B. R. Wood, D. McNaughton, E. G. Stanley, A. G. Elefanty. *Stem Cell Res.* 2010, **4**, 140.

40. M. J. Walsh, A. Hammiche, T. G. Fellous, J. M. Nicholson, M. Cotte, J. Susini, N. J. Fullwood, P. L. Martin-Hirsch, M. R. Alison, F. L. Martin, *Stem Cell Res.* 2009, **3**, 15.

Monitoring *in vitro* Neural Stem Cells Differentiation based on Surfaces–Enhanced Raman Spectroscopy using Gold Nanostars array

Waleed Amed El-Said[1,4], Seung U. Kim[2] and Jeong-Woo Choi[1, 3*]

[1]*Interdisciplinary program of Integrated Biotechnology, Sogang University, 35 Baekbeom-Ro, Mapo-Gu, Seoul 121-742, Republic of Korea*

[2]*Department of Medicine, Faculty of Medicine, University of British Columbia, Vancouver, British Columbia, Canada*

[3]*Department of Chemical and Biomolecular Engineering, Sogang University, 35 Baekbeom-Ro, Mapo-Gu, Seoul 121-742, Republic of Korea*

[4]*Department of Chemistry, Faculty of Science, Assiut University, Assiut, 71516, Egypt*

*Correspondence: Prof. Jeong–Woo Choi

Department of Chemical and Biomolecular Engineering

Sogang University, Seoul, Republic of Korea

Tel. +82–2–705–8480; Fax: +82–2–3273–0331.

E-mail: jwchoi@sogang.ac.kr

Abstract: The development of neurochips for non-invasive monitoring neural stem cells stimulation is highly desirable issue, and can enable the efficient optimization of tissue development protocols. Traditional methods including cell staining and sorting, have long been used, but these techniques are time consuming and may damage cells. Here, we have developed a cell-based chip to monitor the *in-vitro* stepwise differentiation process of embryonic stem cells (ESCs), the one-step differentiation of adult human neural stem cells (HB1.F3), and the electrochemical stimulation of rat pheochromocytoma PC12 cells. Results showed that each cell line exhibited a different behavior during differentiation. The DNA contents changed in an irregular manner during the differentiation of the HB1.F3 cells, while the percentage of proteins increased. In addition, the results revealed that the electrochemical stimulation of PC12 cells induced changes in the synthesis of DNA and proteins. The differentiation of ESCs showed a decrease in some peaks corresponding to the DNA content and an increase in the percentage of protein, in addition to the irregular behavior of some peaks related to both nucleic acids and proteins. The increase in the protein percentage could indicate local variations in protein structure and a maturation shift. These results demonstrate that the SERS technique allows for more rapid biological sample analysis without time-consuming staining, enabling researchers to monitor engineered tissues and optimize culture conditions in a near real time manner.

Keywords: Embryonic neural stem cells; Surface-enhanced Raman spectroscopy; Adult neural stem cells; Differentiation, Electrochemical stimulation.

Introduction

Embryonic stem cells have the ability to differentiate into one of more than 200 cell types, such as neurons, cardiomyocytes, hepatocytes, islet cells, skeletal muscle cells, and endothelial cells.[1] Stem cell therapy could change the treatment of intractable human diseases such as Parkinson's disease, ischemic heart diseases, and diabetes.[2] Neural stem cells (NSCs) have considerable therapeutic potential for the treatment of neurological disorders. The differentiation of NSCs is an important process during the development of the central nervous system.[3] Therefore, monitoring the differentiation of NSCs is of importance in different fields, such as regenerative medicine, transplantable tissue, and as an alternative source of donor tissue neural precursors. Further applications include the repair of pathological processes and the repair of neurodegenerative processes, including Parkinson's and Alzheimer's diseases.[1,4] In addition, understanding the mechanisms of *in-vitro* stem cell differentiation will allow the development of rational approaches to systematically manipulate cell fates. Common methods reported for monitoring the differentiation of neural cells include the reverse transcription polymerase chain reaction (RT-PCR), immunohistochemistry, immunocytochemistry, colorimetric, or sorting techniques.[5] However, these techniques have a number of disadvantages, such as being labor-intensive multistep processes, being endpoint assays that do not offer the

mechanism details, being time consuming, or being destructive methods requiring biomarkers or labels thereby, limiting potential application. The development of an efficient high-throughput, rapid, simple, sensitive, nondestructive and label-free technique for *in-vitro* monitoring of the differentiation of NSCs on a single cell level is therefore needed. This would have an impact on biomedicine as well as on the development of effective stem cell sensors.[6]

Cell-based chips hold great promise for cell-based detection methods, through the use of optical or electrochemical detection systems. Electrochemical cell-based chips allow for easy monitoring and analysis of the cell signals of living cells arising from redox reactions;[7] utilizing several electrochemical techniques such as cyclic voltammetry (CV), differential pulse voltammetry, electric cell-substance impedance sensing (ECIS), scanning electrochemical microscopy (SECM), electrochemical impedance spectroscopy (EIS), and the oxygen electrode.[8] In our previous studies, the voltammetric behaviors of different cancer cells was determined using modified electrodes. These studies reported on the effect of anti-cancer drugs on a cell chip using CV and potential stripping analysis methods.[9] However, the electrochemical behavior of the living cells represented only the cell viability based on electron transfer between the cell and the electrode surface, and the

mechanism of the stem cell differentiation could not be monitored using these electrochemical methods.

Cell-based chips for optical detection have the distinct advantage of being able to visualize changes in cell status.[10] While, white light imaging (phase contrast or differential interference contrast) can reveal the approximate level of *in-situ* differentiation, it is a qualitative technique. Fourier transform infrared (FT–IR) spectroscopy can be used for monitoring the single cell differentiation of fixed or dried stem cells, but is not suitable for monitoring the differentiation of living cells. Although Raman spectroscopy has demonstrated the ability to monitor the differentiation of living NSC, it is too slow to characterize a sufficient number of individual cells to be a reliable clinical technique. Nonetheless, Raman spectroscopy could be used extensively in biomedical research.[11]

The enhancement factors in surface-enhanced Raman spectroscopy (SERS) can be as high as 10^9-10^{15}, which allows this technique to be sensitive enough to detect single molecules.[12] In addition, SERS has 2 to 3 times the sensitivity as compared to fluorescence.[13] As such, the increased sensitivity of Raman scattering has generated tremendous interest in the nanomaterial, spectroscopy, and analytical chemistry communities.[14] SERS offers an exciting opportunity to overcome the critical

disadvantages of the conventional Raman spectroscopy, allowing for relatively lower laser intensity, longer wavelengths, and rapid signal acquisition times. Consequently, near infrared (NIR)-SERS is becoming a useful tool for biological applications[15] with high selectivity and sensitivity, which could extend Raman utility to a wide variety of interfacial systems previously inaccessible to conventional Raman spectroscopy. In addition, the SERS technique gives effective molecule specific information regarding immobilized molecules on the metal surface, *in-situ,* and in aqueous solutions. At present, many researchers continue to demonstrate the great potential of SERS applications in the fields of biochemistry, biophysics, and molecular biology. Average SERS enhanced spectra is one of two strategies to acquire the SERS signals,[16] which are obtained from an ensemble of colloidal particles and aggregates giving a relatively low signal especially before aggregation. Several studies have reported on the use of colloidal metallic (gold (Au) or silver (Ag)) nanoparticles (NPs) or nanorods to perform SERS on living cells and various important biological species such as DNA and protein.[17] Au NPs of different diameters were used as SERS-active agents for monitoring chemical changes during the differentiation of embryonic stem cells (ESCs).[18] However, the non-homogeneity of the NP aggregates caused a dramatic change in the enhancement of Raman signal from one point to another on the cell surface. During the NP preparation some surfactants such as

CTAB (cetyltrimethylammonium bromide) or PVP (polyvinylpyrrolidone) were used.[19] The existence of these species on the metal NP surface results in fewer active sites, and the SERS signal generated by these species could severely interfere with the SERS signals of the target molecules. Samanta et al. (2014) reported on the fabrication of specific targeting SERS nanotags based on the modification of Au NPs with three active Raman reporters and antibodies for the identification of differentiated ESCs.[20] The antibody-conjugated metal NPs could overcome the non-homogeneity limitations of non-targeting NPs. However, the presence of antibodies was reported to cause unwanted SERS signals that were barely distinguishable from the Raman signals originating from target molecules inside the cell.[21] In addition, nuclear-targeted Au NPs have been used as intracellular probes to monitor the differentiation of ESCs using SERS.[22] This was a challenge, due to the existence of several cellular barriers limiting the delivery of SERS–active colloidal NPs to the cell nucleus.[23] Moreover, Au NPs–targeting of the cell nucleus has been reported to influence cellular function, causing DNA damage, cell death, and apoptosis.[24]

The development of SERS-active surfaces has been based on the existence of particular hot spots (Ag or Au nanostructures) on modified substrates, which permits the detection of a few molecules with fluctuating spectral characteristics.[25] However, the

fabrication of SERS-active substrates has been found to create a number of problems, including poor signal enhancement, uniformity, and reproducibility. In previous work conducted by our group, we developed different SERS-active surfaces to monitor anticancer effects as well as to analyze intracellular states.[26, 27] An advanced method for the fabrication of SERS-active surfaces is still required for more effective enhancement of Raman signals.

The present work represents the development and application of an Au nanostructures modified ITO substrate as a SERS-active surface, cell culture system, and working electrode, as shown in Scheme 1. These provide a quantitative, label-free, biocompatible, and noninvasive optical spectroscopy technique for monitoring the *in-vitro* stepwise differentiation process of ESCs, the one-step differentiation of adult human neural stem cells (HB1.F3), and the electrochemical stimulation of rat pheochromocytoma PC12 cells. Thus, the approach described in this paper plays a vital role in identifying the cell types in biomedical stem cell research, overcoming the limitations of the SERS-NPs-based approach. Moreover, this technique is a promising noninvasive tool to monitor the changes in the chemical composition of NSCs during their differentiation, and has potential applications in high throughput analysis, drug screening, and induced pluripotent stem cell generation.

Experimental Section

Materials. Hydrogen tetrachloroaurate (III) trihydrate ($HAuCl_4 \cdot 3H_2O$, 99.9+ %), and phosphate buffered saline (PBS) (pH 7.4, 10 mM) solution were purchased from Sigma-Aldrich (St. Louis, MO, USA). Neurite growth factor (NGF) was obtained from Millipore. Polyethylene glycol-200 (PEG) (MW = 200) was obtained from Yakuri Pure Chemicals Co. Ltd. (Osaka, Japan). All other chemicals used in this study were obtained commercially as reagent grade chemicals. All aqueous solutions were prepared using deionized water (DIW) deionized with a Millipore Milli-Q water purifier operating at a resistance of 18 MΩ cm.

Cell culture. Rat neural PC12 cells, ES cells and HB1.F3 were cultured in DMEM supplemented with 10% heat inactivated fetal bovine serum (FBS; Gibco, Carlsbad, CA, USA) and 1% antibiotics (Gibco). The cells were maintained under standard cell culture conditions at 37 °C in an atmosphere of 5 % CO_2. The medium was changed every two days. The number of cells was determined by the trypan blue assay with a hemacytometer.

Electrochemical measurements. All electrochemical experiments were performed using a potentiostat (CHI-660, CH Instruments, USA) controlled by general-purpose

electrochemical system software. A homemade three-electrode system consisting of cell/Au nanostars/ITO as the working electrode, a platinum wire as the counter electrode and Ag/AgCl as the reference electrode was set up. Measurements were carried out to study the electrical properties of living cells under normal laboratory conditions. PBS (10 mM, pH 7.4) was used as an electrolyte at a scan rate of 50 mV/s.

Raman spectroscopy. The biochemical composition of the control PC12, HB1.F3 and ES cells, as well as the effect of one step differentiation on PC12 cells and HB1.F3 cells or of stepwise differentiation of ES cells were investigated based on the SERS technique using Raman NTEGRA spectra (NT-MDT, Russia) equipped with an inverted optical microscope and a liquid nitrogen-cooled CCD detector. The maximum scan-range, XYZ, was 100 μm × 100 μm × 6 μm, and the resolution of the spectrometer in the XY plane was 200 nm and along the Z axis was 500 nm. Raman spectra were recorded using an NIR laser emitting light at a wavelength of 785 nm with an irradiation laser power of 3 mW on the sample plane. The medium was removed and the cells were washed three times with PBS, which was used during the SERS measurements for eliminating the effect of the medium on SERS signals. Ten scans of 5 s from 600-1750 cm^{-1} were recorded and the mean result was used. A blank spectrum was acquired prior to each step, which allowed the absorbance to be subsequently measured.

Fabrication of gold nanostars array modified ITO substrate. Au nanostars arrays were electrochemically deposited onto ITO substrates (20 mm × 10 mm) using different concentrations of a $HAuCl_4$ aqueous solution containing 20 µL/mL of PEG-200 as a surfactant, according our previously reported method.[27] The, ITO-coated glass substrates were typically cleaned by sequential sonication in 1% Triton X-100 solution, DIW, and ethanol for 15 min, followed by sonication in basic piranha solution (1:1:5, H_2O_2:NH_3:H_2O) for 30 min at 80 ºC. Finally, the substrates were rinsed with DIW and dried under a N_2 stream to obtain a clean ITO surface. Au nanostar arrays were electrochemically deposited onto the ITO substrates by using different concentrations of $HAuCl_4$ (0.3, 0.5 and 0.7 mM) under a constant potential of -1.3 V (vs. Ag/AgCl), and the deposition temperature was controlled and maintained at 25 ºC in an electric-heated thermostatic water bath. To remove any trace surfactants adsorbed on the Au nanostars modified ITO surface, the substrates were rinsed in DIW then boiled for 5 min with isopropyl alcohol under a N_2 stream. The active area for electrochemical deposition of the Au nanostars was 10 x 10 mm, and their surface morphologies were analyzed using a scanning electron microscope (SEM) (ISI DS-130C, Akashi Co., Tokyo, Japan), as shown in Figure 1.

SERS Monitoring of the Differentiation of ES Cells. To monitor the differentiation of the ES cells, approximately 2 × 10^4 mouse ES cells were assembled on an Au nanostars/ITO substrate surface (20 mm x 10 mm) for 28 days. The cells were examined at 14 time points, beginning with the Raman spectrum for adhered cells (day 0), and then every 48 hrs after the cell had adhered to the surface of the substrate. SERS mapping was been conducted for each cell, and the Raman spectrum from 20 points was extracted. The mean Raman spectrum of each observed time point during mouse ES cells differentiation is offset and overlaid in Figure 6.

In-vitro PC12 Electrochemical Stimulation. Electrochemical stimulation of the neurite outgrowth of PC12 was developed based on a previously reported method.[28] Typically, PC12 cells were assembled onto an Au nanostars/ITO substrate at a density of 2 x 10^4 cells/cm^2, then incubated for 24 h to permit attachment and spreading. The PC12 cells were subjected to a steady potential of 100 mV for 2 h. For electrical stimulation, the Au nanostars/ITO served as the anode, an Au wire placed at the opposite end (along the length) of the well served as the cathode and an Ag wire served as a quasi-reference electrode. The cells were maintained in a CO_2 incubator for the duration of the electrical stimulation. After the electrical stimulation, the cells were incubated for an additional 24

h (for a total of 48 h from the start of the experiment). Using SEM, the lengths of the neuritis of the cells under stimulation were compared with controls to estimate the extent of differentiation.

Results and Discussion

Development of Gold nanostars/ITO substrate

Au nanostars are biocompatible nanoconstructs that represent a promising nanoplatform for various biomedical applications, such as SERS,[29] photodynamic therapy,[30] photothermal therapy,[31] photoacoustic imaging,[32] and biosensing.[33] In this study, Au nanostar modified ITO substrates were developed by reduction of $HAuCl_4$, using electrochemical deposition in the presence of PEG-200 as a structure directing agent. Figures 1 (a-c) show SEM images of the Au nanostars/ITO substrates prepared using different concentrations of $HAuCl_4$, revealing the formation of Au 3D-nanostructures 40 nm in diameter. The nanostar morphology consists of multiple perpendicular branches within the same plane, but at slightly different angles. In addition, the density of Au nanostructures is increased by increasing the concentration of $HAuCl_4$, as shown in Figures 1 (a-c). Figure 1-d shows the UV-Vis spectra of three Au nanostars/ITO substrates ranging from 350–800 nm. The absorption spectra of the Au

nanostars/ITO substrates demonstrate that Au nanostars have two broad surface plasmon absorption peaks; one at around 553 nm, resulting from transverse electronic oscillation, and the other in the NIR region (704 nm), due to the longitudinal oscillation of conduction band electrons. These two plasmon bands result from the hybridization of the plasmon from branches that act as "hot spots" due to the "lightning rod" effect.[34] Because of the heterogeneous branch morphology, nanostar ensembles probably enable a wider range of LSPR modes, which explains the broadening of the extinction spectra. In addition, the plasmon peak intensity increased with increasing density of the Au nanostars, as the intensity depends on the branch number/length.[34]

SERS Monitoring of the Electrical Stimulation of PC12 Cells

The rat pheochromocytoma PC12 cell line has been reportedly used as a model system for neuronal differentiation by electrical stimulation or treatment with nerve growth factor.[35] In this study, we used the PC12 cell line as a model system for neuronal differentiation by electrical stimulation, by applying a steady potential of 100 mV for 2 h to the cells. The SEM technique was used to confirm the differentiation of PC12. Figure 2b shows SEM image of control PC12 and also the show SEM images of PC12 after cell stimulation were showed in Figures 2c & 2d, which demonstrate the changes in

morphology and the apparent enlargement of neurons extending from the cell body after cell stimulation. The Raman spectrum of the control PC12 is shown in Figure 2a, which shows Raman peaks at 775 cm^{-1} (Trp, U, C and T), 1001 cm^{-1} (Phe), 1092 cm^{-1} (PO_2^-), 1205 cm^{-1} (Phe and Trp), 1230 cm^{-1} (amide III and T), 857 cm^{-1} (Tyr), 1490 cm^{-1} (G and A) and 1620 cm^{-1} (C=C Trp and Tyr str.).[36] Moreover, the peak at 1270 cm^{-1} corresponds to the presence of amide III and catecholamines such as dopamine (DA). The Raman peak at 1557 cm^{-1} was assigned to C=C str. of a phenyl group. These data corresponds to earlier published cell spectra.[37] On the other hand, the Raman spectrum of the differentiated PC12 cells exhibit changes in several Raman peaks. These changes included a decrease in the Raman peak intensities at 1001 cm^{-1} (Phe), and 1170 cm^{-1} (pro, C−C/C−N str.). Conversely, the intensities of the Raman peaks at 775 cm^{-1} and 1097 cm^{-1} (PO_2^- of nucleic acids) increased after cell differentiation. Moreover, new Raman peaks appeared at 857 cm^{-1} (Tyr), 875 cm^{-1} (lipids, C−C−N^+ str. and carbohydrate C−O−C ring), 1450 cm^{-1} (carbohydrate δCH_2), and 1490 cm^{-1} (nucleic acids, G and A). On the other hand, the Raman peak at 1470 cm^{-1} (pro. def CH) was disappeared after the differentiation of PC12. These results illustrate the ability of the SERS-active surface to monitor the differentiation of PC12 cells. In addition, the electrical stimulation of the PC12 cells induces changes in DNA and protein synthesis.

SERS Monitoring the Differentiation of HB1F3 Cells

The SERS technique was also applied to monitor the differentiation of HB1.F3 cells as shown in Figure 3. Figure 3 exhibit a typical Raman peaks including characteristic peaks corresponding to nucleotide and sugar-phosphate backbone vibrations such as peak at 690 cm^{-1} (DNA, G), 796 cm^{-1} (PO_2^- in DNA, U, C and T), 1310 cm^{-1} (A) and 838 cm^{-1} (PO_2^- in RNA). The protein contents were dominated by Raman peaks corresponding to amide II (1540 cm^{-1}), 913 (Ring str. CC), 955 (str. CC α-helix), 1120 (CN str.), 1155 (CC/CN str.), 1214 cm^{-1} (amide III β-sheet) and 1284 cm^{-1} (amide III) vibrations. Amino acids could be identified by peaks corresponding mainly to phenyl groups, such as Phe (1001 cm^{-1}), Trp (730 and 755 cm^{-1}), Trp vibrations (1540 cm^{-1}), Tyr vibrations (838 cm^{-1}) and 1617 cm^{-1} (C=C Trp, Try). The Raman peaks of lipids were present at 730 cm^{-1}, 1452 cm^{-1} (CN str), 1388 cm^{-1} (CH def), and 1097 cm^{-1} (hydrocarbon chains vib.). Carbohydrates were detected by the identification of Raman peaks for sugars, especially the COC vibrations of sugar rings (1047 cm^{-1} and 1284 cm^{-1}), and at 1440 cm^{-1} (dCH_2), 1400 cm^{-1} (dCOO), and 1120 cm^{-1} (CO str. carbohydrate). In comparison to the undifferentiated HB1.F3 cells, the Raman spectrum for differentiated HB1.F3 cells (Figure 3) demonstrated a decrease in Raman peaks intensities at 755 cm^{-1} (A and Trp),

838 cm^{-1} (Tyr and PO_2^- in RNA/DNA), 913 cm^{-1} (pro, Ring str. CC), 955 cm^{-1} (pro, str. CC α-helix), 1155 cm^{-1} (pro, CC/CN str.), 1440 cm^{-1} (carbohydrate, dCH_2) and 1540 cm^{-1} (Trp and amide II). Raman peak intensities at 690 cm^{-1} (DNA, G) and 1120 cm^{-1} (CO str. carbohydrate) increased after cell differentiation. These results indicate that some contents of DNA (A and PO_2^- in DNA) decrease during the differentiation of stem cells; while, G/DNA increases. On the other hand, the percentage of most proteins contents (Trp, Tyr, pro, Ring str. CC, str. CC α-helix, str. pro. CC/CN) decreases, indicating local variations in protein structure.

Cyclic Voltammetry Monitoring the Differentiation of HB1F3 Cells

In addition, a CV technique was used to monitor the differentiation of HB1.F3 cells. The cyclic voltammetric behavior of undifferentiated HB1.F3 cells over the potential range of +0.6 to -0.2 V exhibited a quasi-reversible redox process with a cathodic peak at +0.13 V and an anodic peak at +0.25 V. The voltammetric behavior of the cells was recorded for 25 cycles. The results demonstrated that with an increase in the number of CV cycles no change in the potential peaks could be observed, but there was a slight decrease in peak current (Figure 4a). In addition, the differentiated HB1.F3 cells exhibited quasi-reversible redox behavior with a cathodic peak at +0.13 V and an anodic

peak at +0.21 V. The voltammetric behavior of the cells showed a decrease in the peak current with an increase in number of cycles (Figure 4b). It of note that the differentiate HB1.F3 cells showed a higher current peak than the undifferentiated cells. The peak-peak separation of undifferentiated HB1.F3 cells (120 mV) is more than that of the differentiated HB1.F3 cells (80 mV), indicating higher reversibility of the differentiated HB1.F3 cells than of the undifferentiated HB1.F3 cells (Figure 4c). The high reversibility of differentiated HB1.F3 cells is related to the nature of neurons, in which the membrane potential very rapidly undergoes a large change (hyperpolarization or depolarization). This is in contrast to non-excitable cells, in which the membrane potential is held at a relatively stable value (resting potential).

SERS Analyze of Undifferentiated Living ES Cells

The differentiation process of neural ES cells is characterized by its differentiation over a long period. Thus, the differentiation process was monitored over time as a stepwise process. Figure 5 shows optical images of ES cells during differentiation over 28 days, which illustrate the changes in the morphology and appearance of neurons that extend from the cell body. The length of the neurons increased with increased differentiation time.

Figure 6a shows the Raman spectrum of undifferentiated ESCs, exhibiting characteristic Raman peaks corresponding to nucleotide and sugar-phosphate backbone vibrations. These include the Raman peaks at 1097 cm^{-1} (PO_2^-), 796 cm^{-1} (PO_2^- bonds in DNA, U, C and T) and 824 cm^{-1} (PO_2^- bonds in RNA). Different protein contents were dominated by Raman peaks corresponding to amide II (1570 cm^{-1}), amide III ß-sheet (1214 cm^{-1}) and amide III (1284 cm^{-1}). Moreover, amino acids could be identified by peaks corresponding mainly to phenyl groups, such as Phe 1001 cm^{-1} (C-C ring breathing: Phe/protein), Trp (724 and 762 cm^{-1}), and Tyr vib. (838 and 1570 cm^{-1}). The Raman peaks of lipids present at 724 cm^{-1}, 1452 cm^{-1} (CN str.), 1388 cm^{-1} (CH def.), and 1097 cm^{-1} correspond to vibrations of the hydrocarbon chains. Carbohydrates were also detected by identification of the Raman peaks of sugars, especially the COC vibrations of sugar rings (1051, 1097 and 1284 cm^{-1}), and CH def. at 1388 cm^{-1}. The peak assignments of the spectrum are presented in Table 1.

SERS Real Time Monitoring the Differentiation of ES Cells

Ami et al., (2008) and Zelig et al., (2010) have reported that nucleic acids in undifferentiated cells were decreased in compared to differentiated cells[4]; while, Schulze and his group (2010) have shown high contents of nucleic acids in

undifferentiated cells[38]. On the other hand, some studies have demonstrated that the protein composition[39,40] have been increased compared to differentiated cells have been described[4]. However, such increases have also been also associated with the differentiation process[38].

The SERS technique was used as a real time tool to monitor the differentiation on ES cells. The SERS results of ES cells during differentiation (Figure 6b) demonstrated that the intensities of some Raman peaks changed. New peaks appeared while others disappeared during the differentiation of ES cells. The change in the Raman spectrum at several Raman shifts represents varying amounts of biochemical components, including nuclear material, DNA/RNA bases, the DNA backbone, amino acids, proteins, and lipids, as indicated by changes in the intensity of the peaks at 650 (Tyr), 738 (Trp), 828 (Trp and DNA/RNA PO_2), 850 (Trp), 1001 (Phe), 1160 (proteins C-N/C-C str.), 1220 (DNA/RNA bases T and A), 1340 (bases of DNA/RNA G and A), 1580 (proteins (CH) and lipids, bases of DNA/RNA G and A), and at 1617 cm^{-1} (prot, C=C Trp and Tyr).

The behavior of the Raman intensity changes at each peak was monitored. Peaks at 650 cm^{-1} (Tyr) and 1160 cm^{-1} (pro, CN/CC star.) appeared after the cells had adhered to the substrate for two weeks, and the intensity increased with culture time, as shown in Figures 7a & 7b. Figures 7c and 7d demonstrate that the intensities of the Raman peaks at

738 cm^{-1} (Trp) and 1617 cm^{-1} (pro, (C=C Trp and Tyr)) increased with culture time, which indicates that the percentage of these protein components increased as culture time increased. However, these peaks disappeared after two weeks. Similarly, Figure 8a shows that the intensity of the Raman peak at 828 cm^{-1} (Trp and to DNA/RNA PO_2) increased with culture time for two weeks and then disappeared. The Raman peak intensities at 850 cm^{-1} (Trp), 1220 cm^{-1} (bases of DNA/RNA (T and A) and proteins (amid III)), and 1340 cm^{-1} (bases of DNA/RNA G and A) changed irregularly with culture time, as shown in Figures 8b-d. In addition, the Raman peak intensity at 1001 cm^{-1} (Phe) decreased with culture time (Figure 9a). In contrast, Figure 9b demonstrates that the intensity of the Raman peak at 1580 cm^{-1} (bases of DNA/RNA (G and A)) increased with culture time.

Remarkably, the SERS spectra of the differentiated ESCs demonstrated a significant increase in Raman intensities corresponding to some protein components, such as amino acids, Trp, Tyr, and CN/CC (650, 738 and 1617 cm^{-1}) , which increased. On the other hand, the percentage of Phe (1001 cm^{-1}) decreased during the differentiation process. The percentage of the bases of DNA/RNA (G and A) (1580 cm^{-1}) increased with an increase in the differentiation time. In contrast, it was observed that the intensities of the Raman peaks of proteins and DNA were changed in an irregular manner.

Furthermore, Figures 9c & 9d show that the Raman intensities of nucleic acids

(DNA/RNA composites) at 1580 cm^{-1} were divided by protein-related bands, such as 1001 cm^{-1} (Phe) and 1160 cm^{-1} (CN/CC star.). These results indicate that the Raman peaks for the protein/nucleic acid intensity increased, while the peaks for the proteins components decreased.

The percentage of some protein components in the differentiated ES cells increased, while others decreased, as compared to the undifferentiated cells. This was also observed in the percentage of DNA/RNA components as DNA is the original template for protein synthesis. Thus, a change in the DNA may affect synthesis of the protein. Although previous studies have shown an increase in nucleic acids and proteins in differentiated cells as compared to undifferentiated cells,[38] others have shown opposite results.[39] Our results demonstrated an increase in some nucleic acids and proteins, a decrease in some components, and irregular trends in other components during the differentiation process, which is consistent with previous studies.[38, 39]

To verify our results, the change in the total protein content during ESC differentiation was evaluated based on a colorimetric method using a Diamond GPT kit following the manufacturer's instructions. The culture medium was removed, the adhered cells were washed three times with ice-cold PBS buffer, and the PBS was drained off. 100 μl/10^7 cells in chilled RIPA buffer were then added, the adherent cells scraped off, and the cell

suspension kept for 1 hr. Finally, the cell lysate was collected by centrifuging the suspension at 12000 rpm for 20 min at 4 °C. The total protein concentration of the lysate was determined based on a colorimetric test, in which a standard solution was used. The intensity of the specimen was measured against the reagent blank at 546 nm wavelength after 5 min. Figure 10 shows the change in the total protein content as a function of differentiation time, demonstrating that the total amount of protein increased with increasing differentiation time, which is in agreement with the SERS results.

These findings indicate that there is a change in the percentage of total Raman-active biomolecular components during the differentiation of mouse ES cells.

Conclusions

In summary, these results demonstrate that the Raman technique can be used for real time monitoring of the differentiation of different neural cells (PC12 cells, embryonic stem cells and adult stem cells). Each cell line has a different behavior during differentiation. The differentiation of neural ES cells could be analyzed with time, as it is a stepwise process, which is a challenge in the tissue engineering filed. These results also demonstrate that the DNA content seems to change irregularly during the differentiation of stem cells. The percentage of most proteins components increased, while that of some

proteins components decreased. The increase in the amount of proteins reflects local variations in protein structure and a maturational shift. The results also indicate that the electrostimulation of PC12 cells induces changes in the synthesis of DNA and proteins. The differentiation of ES cells showed irregular changes in DNA content and an increase in protein percentage, in addition to the irregular behavior of some peaks related to both nucleic acids and proteins. Furthermore, the differentiated HB1.F3 cells showed higher reversibility more than the undifferentiated HB1.F3 cells. Therefore, the SERS analysis technique allows for more rapid sample analysis without time-consuming staining.

Acknowledgment

This work was supported by the Leading Foreign Research Institute Recruitment Program through the National Research Foundation of Korea (NRF) funded by the Ministry of Science, ICT & Future Planning (MSIP) (2013K1A4A3055268) and by the National Research Foundation of Korea (NRF) grant funded by the Korea government (MSIP) (2014R1A2A1A10051725).

Table 1. Peak assignments of control ES cell SERS spectrum

Raman shift cm^{-1}	Assignment			
	Proteins	Lipids	Nucleic Acids	carbohydrates
1611	C=C Try, Trp			
1570	Amide II, Trp , Phe, Tyr		G, A	
1498			G, A	
1422			A, G	
1388		CH def		CH def
1323	CH_3CH_2 twist		A, G	
1284	amide III			C-O str.
1214	Amide III βsheetTryp, Phy str.		T, A	
1097		Chain C-C str.	PO_2^- str.	C-O-C glycos.
1051				C-O str.
1001	Sym. Ring br Phe			
960	proteins: ν(CC)			
918	Pro.: ring ν(CC)			
838	Ring br. Tyr		O-P-O asym. str.	
796			O-P-O str. DNA, U,C,T ring br	
762	Ring breath Trp			
724	Ring br. Trp	C-N head group	A	

Figure Captions

Scheme 1. Schematic diagram for fabrication of neural stem cell-based chip and its applications as cell culture system for SERS/electrochemical monitoring of the stem cell differentiation process.

Figure 1. SEM image of an Au nanostars modified ITO substrate fabricated using aqueous solution of a $HAuCl_4$ of different concentrations **(a)** 0.3 mM, **(b)** 0.5 mM and **(c)** 0.7 mM containing 20 µL/mL of PEG-200 under a constant potential of -1.3 V (vs. Ag/AgCl), and the deposition temperature was maintained at 25 °C. **(d)** UV-vis spectra of the three Au nanostars/ITO substrates. Scale bar 100 nm.

Figure 2. Electrical stimulation of PC12: (a) Raman spectrum for (1) undifferentiated and (2) differentiated PC12 cells within range of 600 cm^{-1} to 1750 cm^{-1}, **(b)** SEM image of undifferentiated PC12 cell, **(c and d)** SEM images of differentiated PC12 cell.

Figure 3. Raman spectra for (1) undifferentiated HB1.F3 cells and (2) differentiated HB1.F3 cells within range of 600 cm^{-1} to 1750 cm^{-1}.

Figure 4. CV monitoring of the differentiation of HB1.F3 cells **(a)** CV for undifferentiated HB1.F3 cells for 25 cycles, **(b)** CV for differentiated HB1.F3 cells for 25 cycles and **(c)** CV for differentiated and undifferentiated HB1.F3 cells. The cell number was 2.1×10^4 cell/ml. Data represent the mean ± standard deviation of three different experiments. PBS (10 mM, pH 7.4) was used as an electrolyte at a scan rate of 50 mV/s.

Figure 5. Optical images of control ES cells (0 day) **(a)** and after 2 **(b)**, 4 **(c)**, 6 **(d)**, 8 **(e)**, 10 **(f)**, 12 **(g)**, 14 **(h)**, 16 **(i)**, 18 **(j)**, 20 **(k)**, 22 **(l)**, 24 **(m)**, 26 **(n)** and 28 **(o)** days of differentiation process.

Figure 6. SERS spectrum for **(a)** undifferentiated ES Cells and **(b)** Real time monitoring of the differentiated ES cells over 28 days within range of 600 cm^{-1} to 1750 cm^{-1}.

Figure 7. Changes in the intensities of some Raman peaks that characterize the protein contents with culture time at different Raman shifts, **(a)** 650 cm^{-1} (Tyr), **(b)** 1160 cm^{-1} (CN/CC star.), **(c)** 738 cm^{-1} (Trp), and **(d)** 1617 cm^{-1} (C=C Trp and Tyr). Data represents the mean ± standard deviation of ten different points.

Figure 8. Changes in the intensities of some Raman peaks that characterize the nucleic acids percentages with culture time at different Raman shift values: **(a)** 828 cm^{-1} (Trp and to DNA/RNA PO_2), **(b)** 850 cm^{-1} (Trp), **(c)** 1220 cm^{-1} (bases of DNA/RNA (T and A) and proteins (amid III)), and **(d)** 1340 cm^{-1} (bases of DNA/RNA G and A). Data represents the mean ± standard deviation of ten different points.

Figure 9. Changes in the intensities of some characteristic Raman peaks with culture time at different Raman shifts: **(a)** 1001 cm^{-1} (Phe) and **(b)** 1580 cm^{-1} (bases of DNA/RNA (G and A)). Raman intensities of nucleic acids (DNA/RNA composites) divided by protein-related bands, **(c)** 1580 cm^{-1}/1001 cm^{-1} (Phe) and **(d)** 1580 cm^{-1}/1160 cm^{-1} (CN/CC star.). Data represents the mean ± standard deviation of ten different points.

Figure 10. The total protein content changes as a function of differentiation time over 28 days.

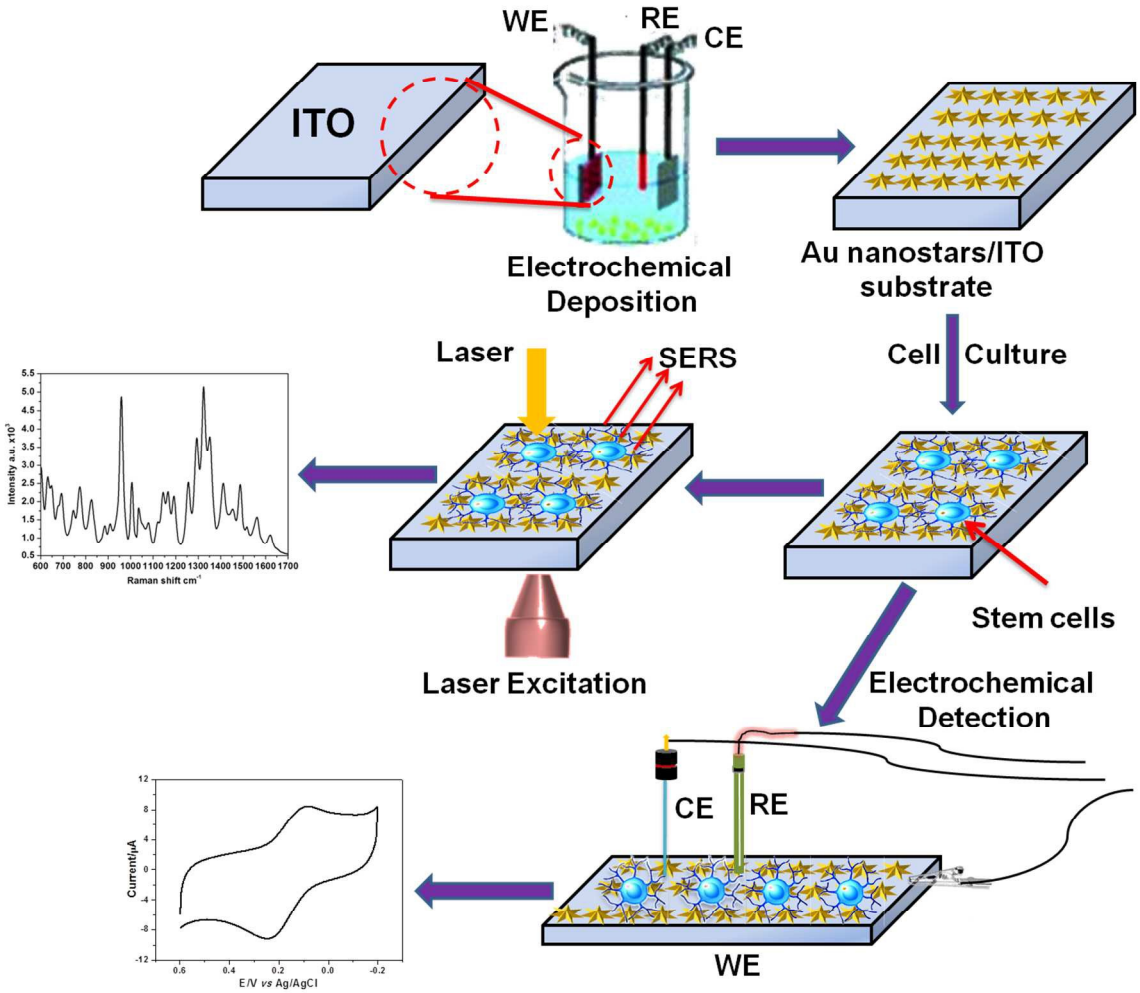

Scheme 1

References

1. B. Coleman, J. B. Fallon, L. N. Pettingill, M. G. de-Silva, R. K. Shepherd, *Experimental Cell Research*, 2007, **2**, 232; K. Takahashi, K. Tanabe, M. Ohnuki, M. Narita, T. Ichisaka, K. Tomoda, S. Yamanaka, *Cell*, 2007, **5**, 861.

2. O. Lindvall, *Pharmacological Research*, 2003, **47** (4) 279.

3. J. Briscoe, B. G. Novitch, *Philos Trans R Soc Lond B Biol Sci*, 2008, **363**, 57.

4. D. Ami, T. Neri, A. Natalello, P. Mereghetti, S.M. Doglia, M. Zanoni, M. Zuccotti, S. Garagna, C.A. Redi, *Biochimica et Biophysica Acta (BBA) - Molecular Cell Research*, 1783 (2008) 98; U. Zelig, Z. Dror, S. Iskovich, A. Zwielly, M. Ben-Harush, I. Nathan, S. Mordechai, J. Kapelushnik, *J. Biomed. Opt.* 2010, **15**, 037008.

5. R. M. Lemoli, F. Bertolini, R. Cancedda, M. De Luca, A. Del Santo, G. Ferrari, S. Ferrari, G. Martino, F. Mavilio, S. Tura, *Haematologica*, 2005, **90**, 360; Y.-S. Hwang, Y. Kang, A. Mantalaris, *Biotechnology and Bioprocess Engineering*, 2007, **12**, 15.

6. J. K. Pijanka, D. Kumar, T. Dale, I. Yousef, G. Parkes, V. Untereiner, Y. Yang, P. Dumas, D. Collins, M. Manfait, G. D. Sockalingum, N. R. Forsyth, J. Sule-Suso, *Analyst*, 2010, **135**, 3126.

7. T.-H. Kim, W. A. El-Said, J.H. An, J.-W. Choi, Nanomedicine: Nanotechnology, Biology and Medicine, 2013, 9 (3), 336; W. A. El-Said, C.-H. Yea, H.H. Kim, J.-W. Choi,

Current Applied Physics, 2009, 9, e76–e80; T.-H. Kim, W. A. El-Said, J.-W. Choi, Biosensors and Bioelectronics, 2012, 32, 266; W. A. El-Said, C.-H. Yea, J.-W. Choi, Il-K. Kwon, Thin Solid Films, 2009, 518, 661; W. A. El-Said, T.-H. Kim, H.C. Kim, J.-W. Choi, Nanotechnology, 2010, 21, 455501 (7pp).

8. A. J. Bard, X. Li, W. Zhan, *Biosensors and Bioelectronics*, 2006, **4**, 461; H. Lu, M. Gratzl, *Analytical Chemistry*, 1999, **14**, 2821; H. F. Cui, J. S. Ye, Y. Chen, S. C. Chong, F. S. Sheu, *Analytical Chemistry*, 2006, **18**, 6347; R. J. Fasching, S.-J. Bai, T. Fabian, F. B. Prinz, *Microelectronic Engineering*, 2006, **4–9**, 1638; T. Kaya, Y. S. Torisawa, D. Oyamatsu, M. Nishizawa, T. Matsue, *Biosensors and Bioelectronics*, 2003, **11**, 1379; S. Kasai, H. Shiku, Y. Torisawa, K. Nagamine, T. Yasukawa, T. Watanabe, T. Matsue, *Analytica Chimica Acta*, 2006, **1**, 55; S. Kasai, H. Shiku, Y. Torisawa, K. Nagamine, T. Yasukawa, T. Watanabe, T. Matsue, *Analytica Chimica Acta*, 2006, **1**, 55; P. Wolf, A. Rothermel, A. G. Beck-Sickinger, A. A. Robitzki, *Biosensors and Bioelectronics*, 2008, **2**, 253.

9. W. A. El-Said, C.H. Yea, H.H. Kim, B.K. Oh, J.-W. Choi, *Biosensors and Bioelectronics*, 2009, **5**, 1259.

10. X. Michalet, F. F. Pinaud, L. A. Bentolila, J. M. Tsay, S. Doose, J. J. Li, G. Sundaresan, A. M. Wu, S. S. Gambhir, S. Weiss, *Science*, 2005, **5709**, 538; R. P. Singh,

B.K. Oh, K. K. Koo, J. Y. Jyoung, S. Jeong, J.W. Choi, *Biochip Journal*, 2008, **4**, 223; L. Zhu, W. Wu, M. Q. Zhu, J. J. Han, J. K. Hurst, A. D. Li, *J. Am. Chem. Soc.*, 2007, **12**, 3524.

11. A. Downes, R. Mouras, A. Elfick, *J Biomed Biotechnol*, 2010, **2010**, 101864.

12. W. E. Doering, and S. M. Nie, *J. Phys. Chem. B.* 2002, **106** (2), 311; S. Nie, S. R. Emory, *Science*, 1997, **275** (5303), 1102.

13. K. Flauds, R. P. Barbagallo, J. T. Keer, W. E. Smith, D. Graham, *Analyst*, 2004, **129**, 567; Y. C. Cao, R. Jin, C. A. Mirkin, *Science*, 2002, **297**, 1536.

14. M. Moskovits, *J. Raman Spectroscopy*, 2005, **36** (6-7), 485; K. Kneipp, H. Kneipp, I. Itzkan, R. R. Dasari, M. S. Feld, *J. Phys. Cond. Matter.* 2002, **14** (18), R597; W. A. El-Said, J.-W. Choi, *Biotechnology and Bioprocess Engineering*, 2014, **19** (6), 1069.

15. M. Volkan, D. L. Stokes, T. Vo-Dinh, *Appl. Spectrosc.* 2000, **54**, 1842.

16. R. Aroca, Surface-Enhanced Vibrational Spectroscopy; John Wiley & Sons, U.K. (2006).

17. K. Kneipp, A. S. Haka, H. Kneipp, K. Badizadegan, N. Yoshizawa, C. Boone, K. E. Shafer-Peltier, J. T. Motz, R. R. Dasari, M. S. Feld, *Appl. Spectrosc.* 2002, **56**, 150; H. W. Tang, X. B. Yang, J. Kirkham, D. A. Smith, *Appl. Spectrosc.* 2008, **62**, 1060; X. Huang, I. H. El-Sayed, W. Qian, M. A. El-Sayed, *Nano Lett.* 2007, **7**, 1591; H. Morjani, J. F. Riou, I.

Nabiev, F. Lavelle, M. Manfait, *Cancer Res.* 1993, **53**, 4784; M. Manfait, H. Morjani, I. Nabiev, *J. Cell. Pharmaco.* 1992, **3**, 120.

18. B. Moody, C. M. Haslauer, E. Kirk, A. Kannan, E. G. Loboa, G. S. McCarty, *Appl. Spectrosc.* 2010, **64**, 1227–1233; R. R. Sathuluri, H. Yoshikawa, E. Shimizu, M. Saito, E. Tamiya, *PLoS ONE*, 2011, **6**, e22802.

19. S. Ayyappan, R. S. Gopalan, G. N. Subbanna, C. N. R. Rao, *J. Mater. Res.* 1997, **12**, 398; C. J. Johnson, E. Dujardin, S. A. Davis, C. J. Murphy, S. Mann, *J. Mater. Chem.* 2002, **12**, 1765.

20. A. Samanta1, R. K. Das, S. J. Park, K. K. Maiti, Y. T. Chang, *Am. J. Nucl. Med. Mol. Imaging*, 2014, **4(2)**, 114-124.

21. M.-D. Li, Y. Cui, M.-X. Gao, J. Luo, B. Ren, Z.-Q. Tian, *Anal. Chem.* 2008, **80**, 5118.

22. A. Huefner, W.-L. Kuan, R. A. Barker, S. Mahajan, *Nano Lett.* 2013, **13**, 2463−2470

23. A. G. Tkachenko, H. Xie, D. Coleman, W. Glomm, J. Ryan, M. F. Anderson, S. Franzen, D. L. Feldheim, *JACS*, 2003, **125**, 4700.

24. Kang B, Mackey MA, El-Sayed MA , J. Am. Chem. Soc. 2010, 132, 1517–1519.

25. E. C. Le Ru, , E. Blackie, M. Meyer, P. G. Etchegoin, *J. Phys. Chem. C*, 2007, **111**, 13794; P. G. Etchegoin, M. Meyer, E. Blackie, E. C. Le Ru, *Anal. Chem.* 2007, **79**, 8411.

26. W. A. El-Said, H.-Y. Cho, C.-H. Yea, J.-W. Choi, *Advanced Materials*, 2014, **26** (6),

910; W. A. El-Said, T.-H. Kim, H.C. Kim, J.-W. Choi, *PLoS ONE*, 2011, 6(2): e15836; W. A. El-Said, T.-H. Kim, Y.-H. Chung, J.-W. Choi, *Biomaterials*, 2015, **40**, 80.

27. W. A. El-Said, T.-H. Kim, H. Kim, J.-W. Choi, *Biosensors and Bioelectronics*, 2010, **26**, 1486.

28. C. E. Schmidt, V. R. Shastri, J. P. Vacanti, R. Langer, *Proceedings of the National Academy of Sciences*, 1997, **94**, 8948.

29. Rodriguez-Lorenzo L, Alvarez-Puebla RA, Pastoriza-Santos I, Mazzucco S, Ste phan O, Kociak M, Liz-Marzan LM, Garcia de Abajo FJ. J Am Chem Soc. 2009; 131:4616; Barbosa S, Agrawal A, Rodriguez-Lorenzo L, Pastoriza-Santos I, Alvar ez-Puebla RA, Kornowski A, Weller H, Liz-Marzan LM. Langmuir. 2010; 26:1494 3; Lu W, Singh AK, Khan SA, Senapati D, Yu H, Ray PC. J Am Chem Soc. 2 010; 132:18103; Su Q, Ma X, Dong J, Jiang C, Qian W. ACS Appl Mater Interf aces. 2011; 3:1873; Schutz M, Steinigeweg D, Salehi M, Kompe K, Schlucker S. Chem Comm. 2011; 47:4216.

30. Fales AM, Yuan (co-first author) H, Vo-Dinh T. Langmuir. 2011; 27:12186.

31. Van de Broek B, Devoogdt N, D'Hollander A, Gijs HL, Jans K, Lagae L, Muyldermans S, Maes G, Borghs G. ACS Nano. 2011; 5:4319; Yuan H, Khoury CG, Wilson CM, Grant GA, Bennett AJ, Vo-Dinh T. Nanomedicine: NBM.

201210.1016/j.nano.2012.02.005; Yuan H, Fales AM, Vo-Dinh T. J Am Chem Soc. 2012; 134:11358.

32. Kim C, Song HM, Cai X, Yao J, Wei A, Wang LV. J Mater Chem. 2011; 2 1:2841.

33. Dondapati SK, Sau TK, Hrelescu C, Klar TA, Stefani FD, Feldmann J. ACS Nano. 2010; 4:6318.

34. Yuan H, Khoury CG, Hwang H, Wilson CM, Grant GA, Vo-Dinh T. Nanotec hnology. 2012; 23:075102.

35. D. R. Kaplan, R. M. Stephens, *J Neurobiol*, 1994, **25**, 1404; E. Bieberich, A. Guiseppi-Elie, *Biosensors and Bioelectronics*, 2004, **19**, 923.

36. I. Notingher, S. Verrier, S. Haque, J. M. Polak, L. L. Hench, *Biopolymers*, 2003, **72**, 230.

37. R. J. Dijkstra, W. J. J. M. Scheenen, N. Dam, E. W. Roubos, J. J. ter Meulen, *J. Neurosci. Methods*, 2007, **159**, 43.

38. H. G. Schulze, S. O. Konorov, N. J. Caron, J. M. Piret, M. W. Blades, R. F. B. Turner, *Anal. Chem*. 2010, **82**, 5020; W. Tanthanuch, K. Thumanu, C. Lorthongpanich, R. Parnpai, P. Heraud. *J. Mol. Struct.* 2010, **967**, 189; S. O. Konorov, H. G. Schulze, C. G. Atkins, J. M. Piret, S. A. Aparicio, R. F. B. Turner, M. W. Blades, *Anal. Chem.* 2011, **83**,

6254; A. Huefner, W.-L. Kuan, R. A. Barker, S. Mahajan, *Nano Lett.* 2013, **13**, 2463.

39. P. Heraud, E. S. Ng, S. Caine, Q. C. Yu, C. Hirst, R. Mayberry, A. Bruce, B. R. Wood, D. McNaughton, E. G. Stanley, A. G. Elefanty. *Stem Cell Res.* 2010, **4**, 140.

40. M. J. Walsh, A. Hammiche, T. G. Fellous, J. M. Nicholson, M. Cotte, J. Susini, N. J. Fullwood, P. L. Martin-Hirsch, M. R. Alison, F. L. Martin, *Stem Cell Res.* 2009, **3**, 15.

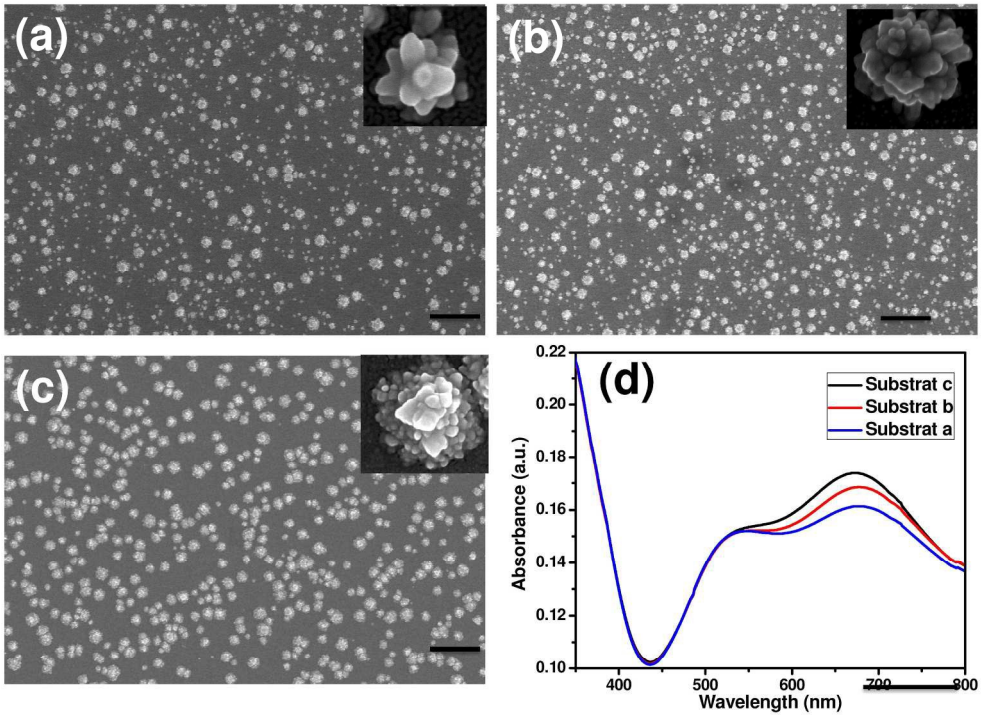

215x166mm (300 x 300 DPI)

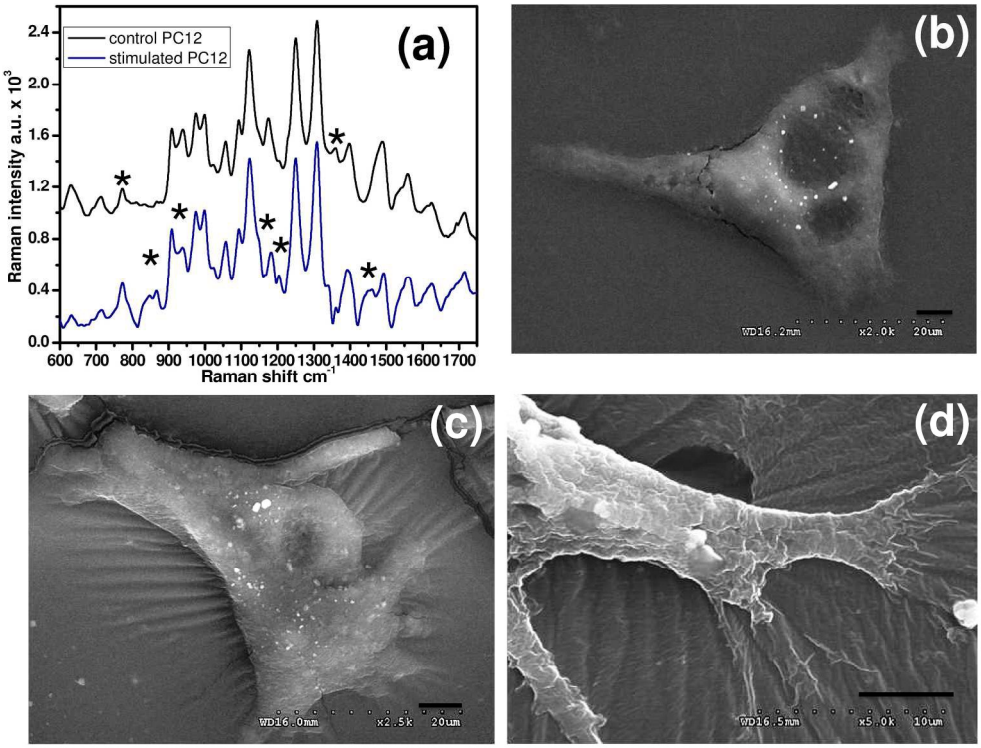

215x166mm (300 x 300 DPI)

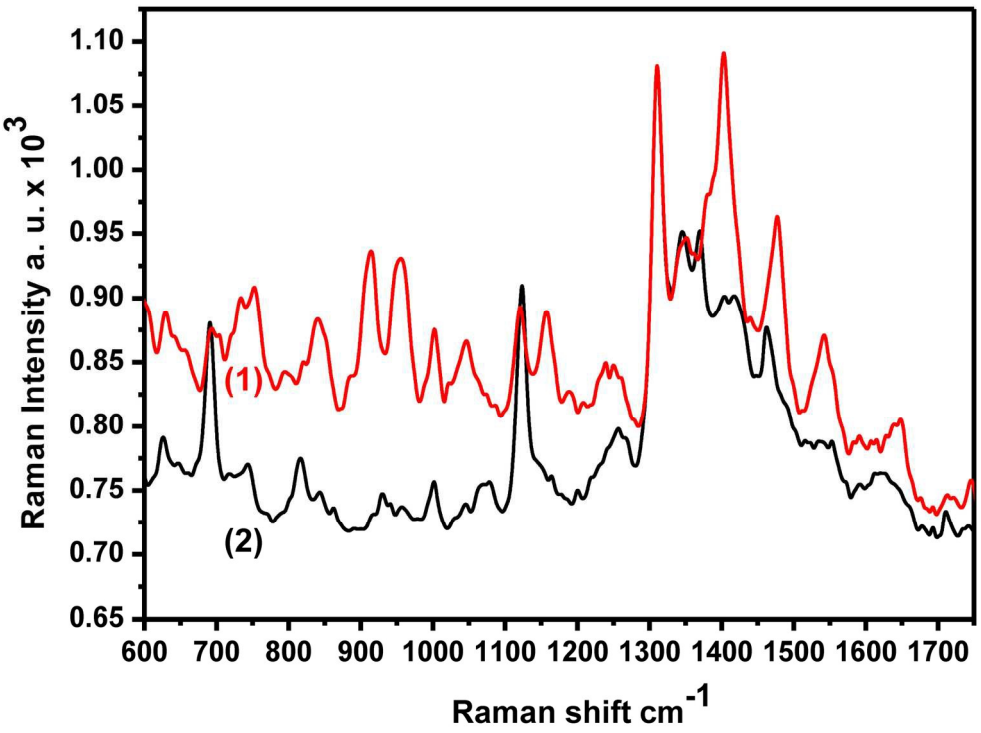

161x119mm (300 x 300 DPI)

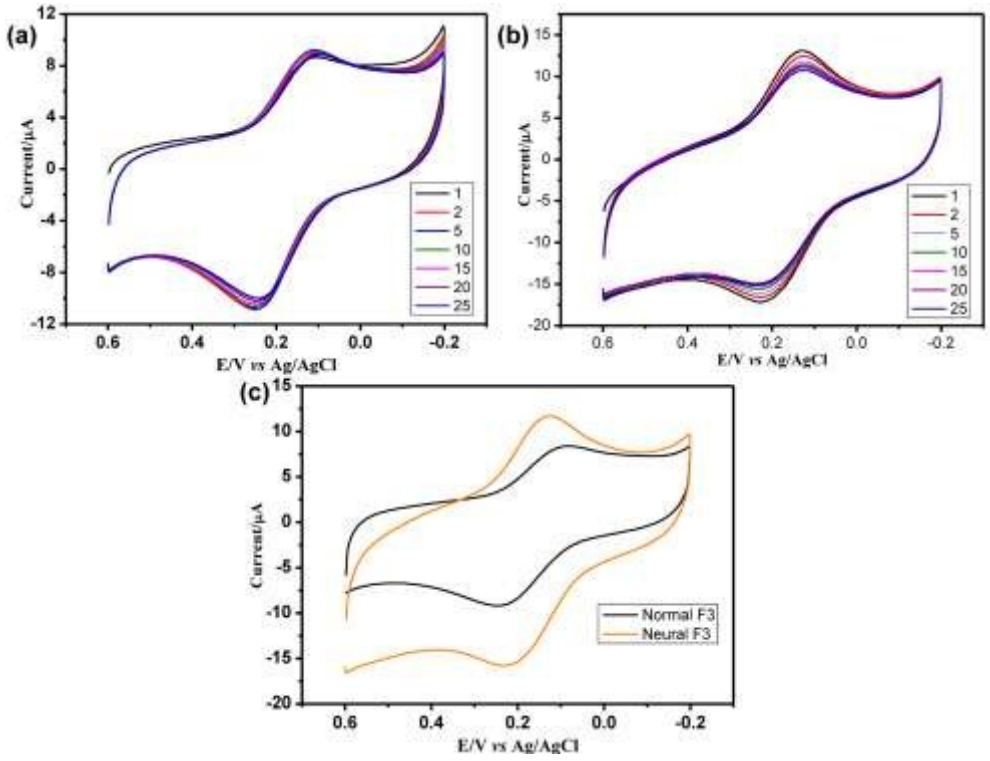

190x142mm (300 x 300 DPI)

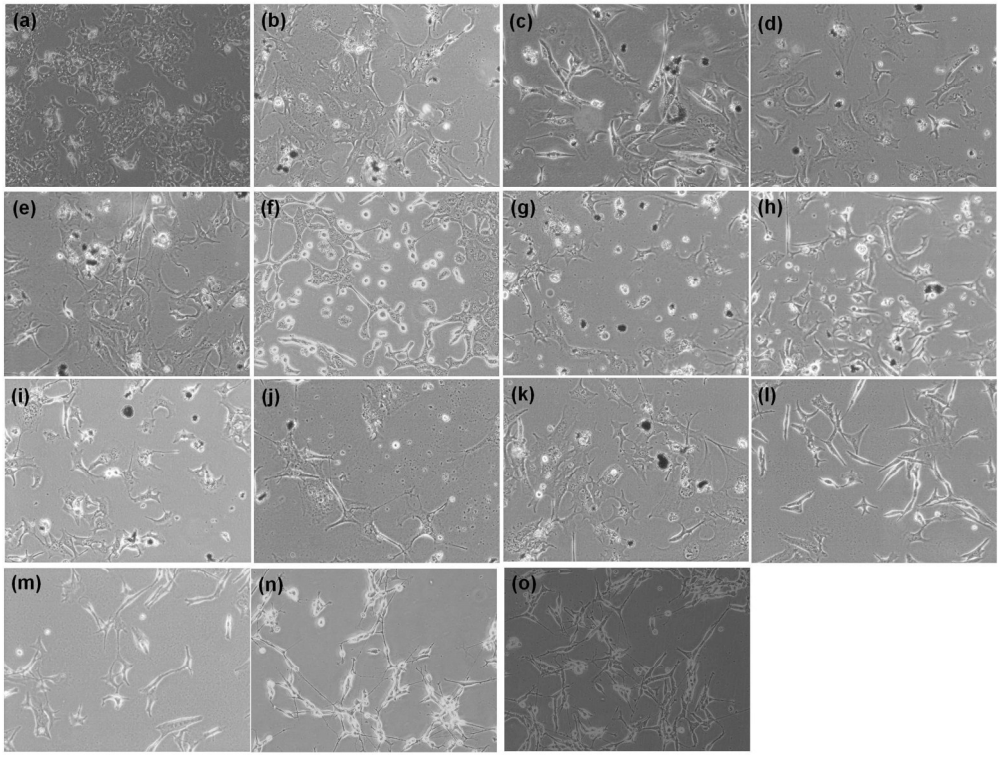

215x166mm (300 x 300 DPI)

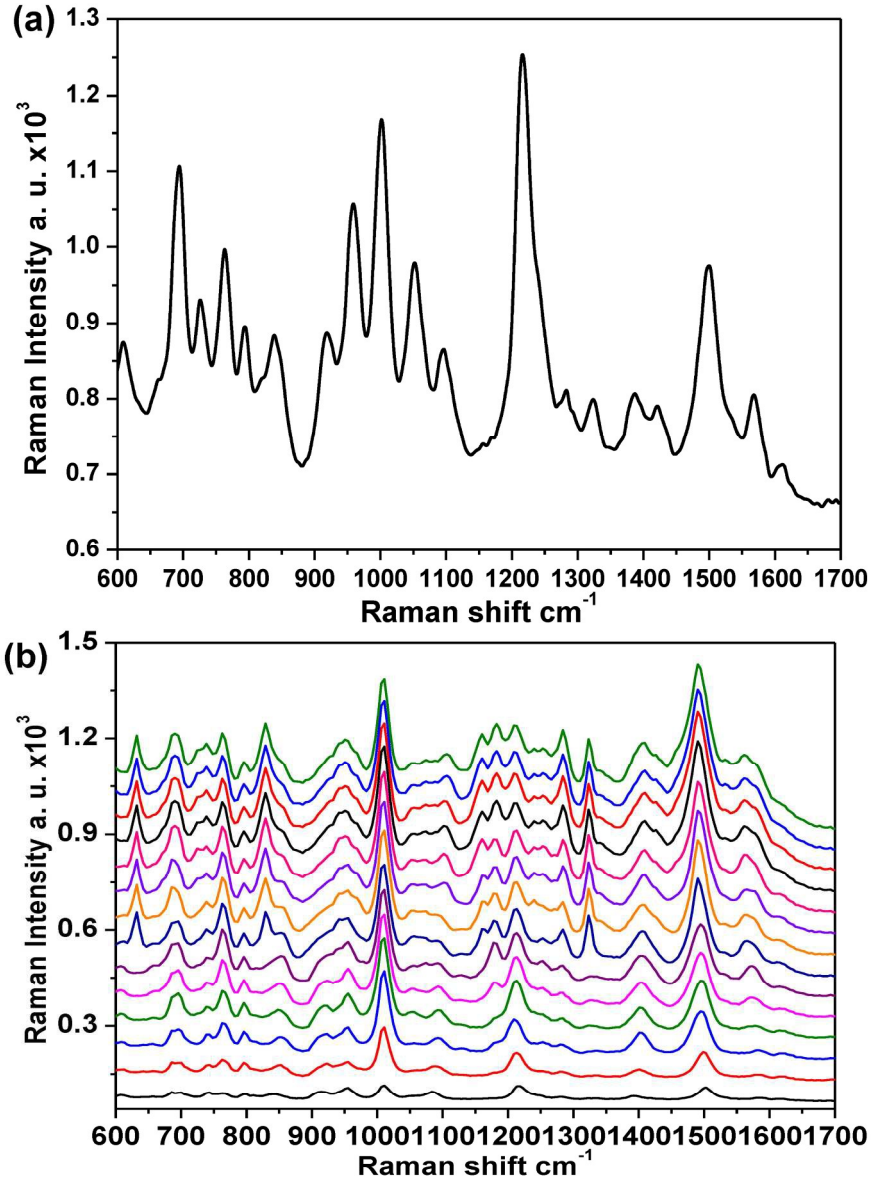

190x254mm (300 x 300 DPI)

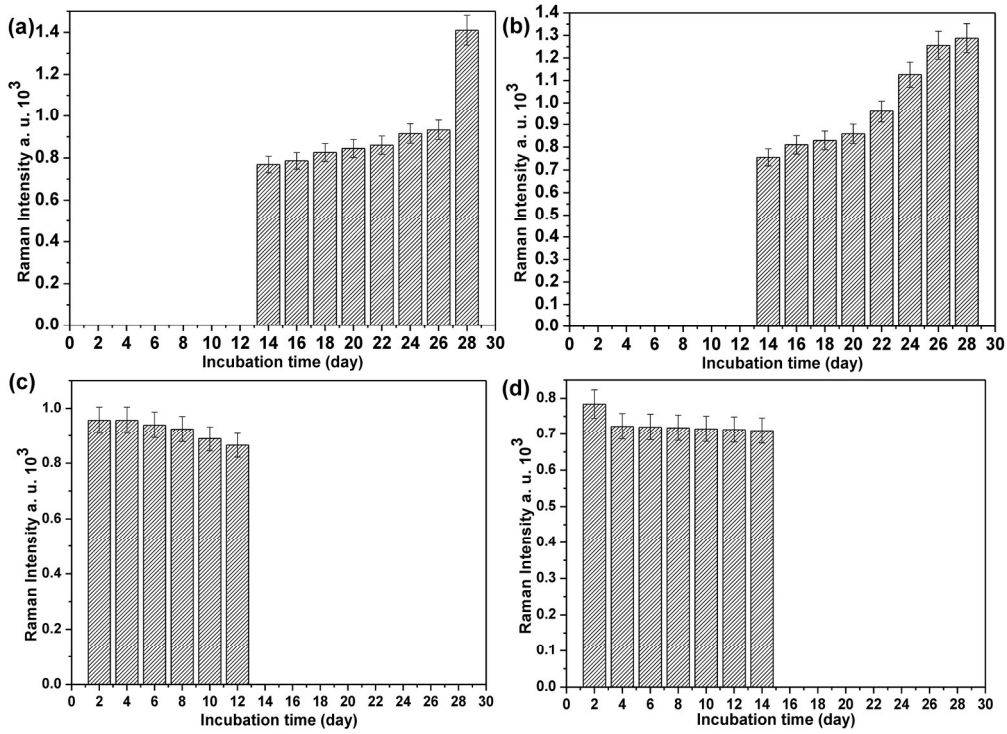

190x142mm (300 x 300 DPI)

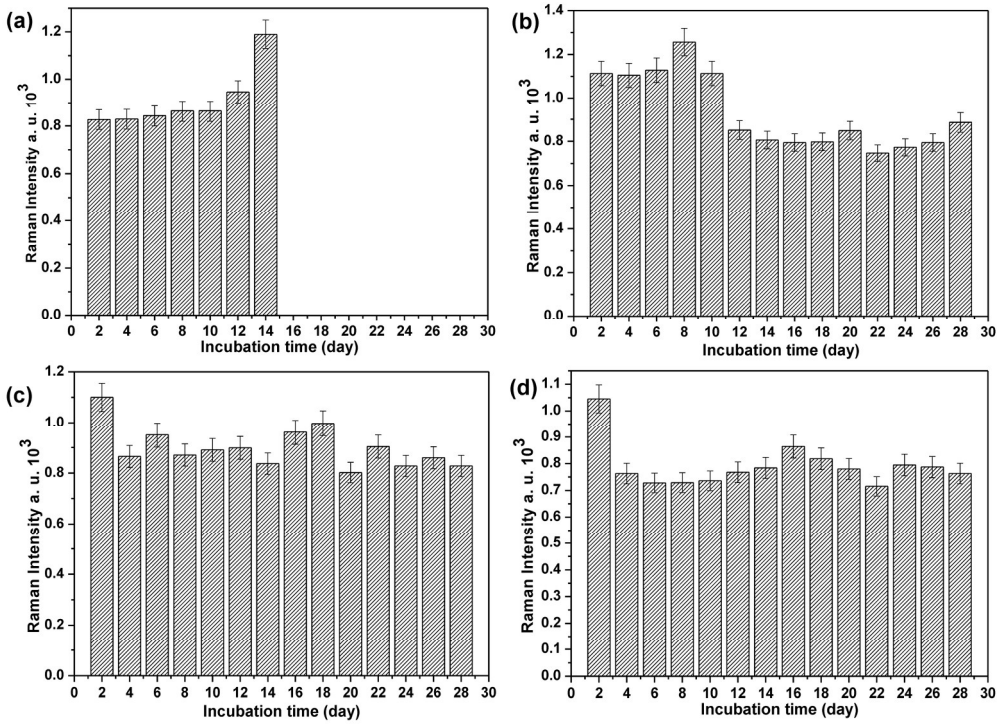

190x142mm (300 x 300 DPI)

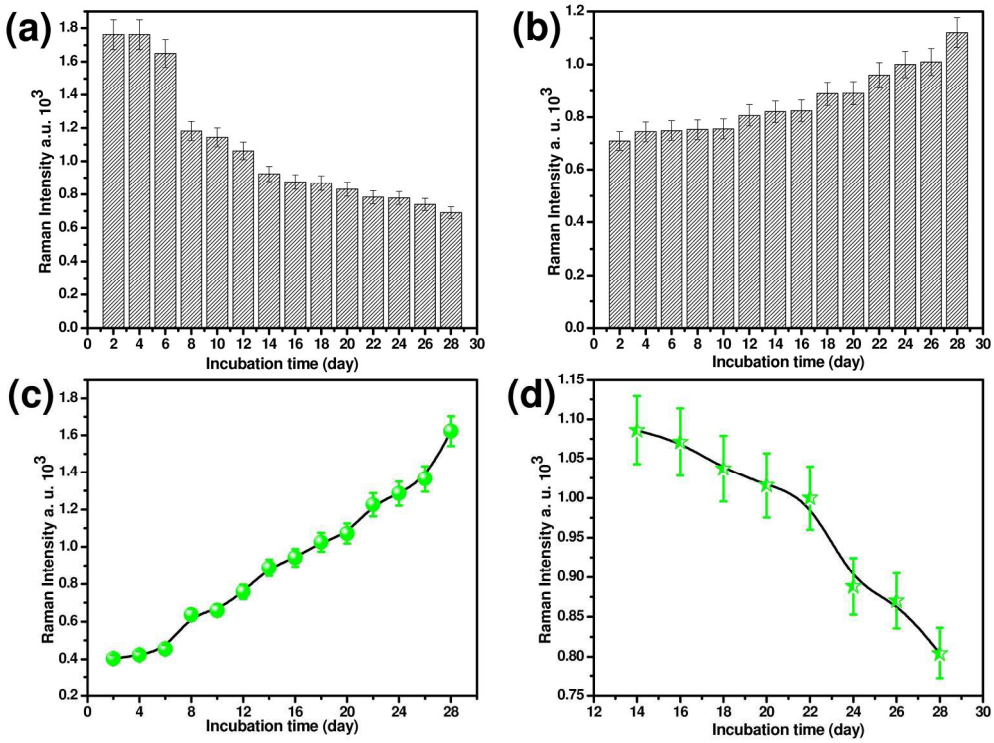

215x166mm (300 x 300 DPI)

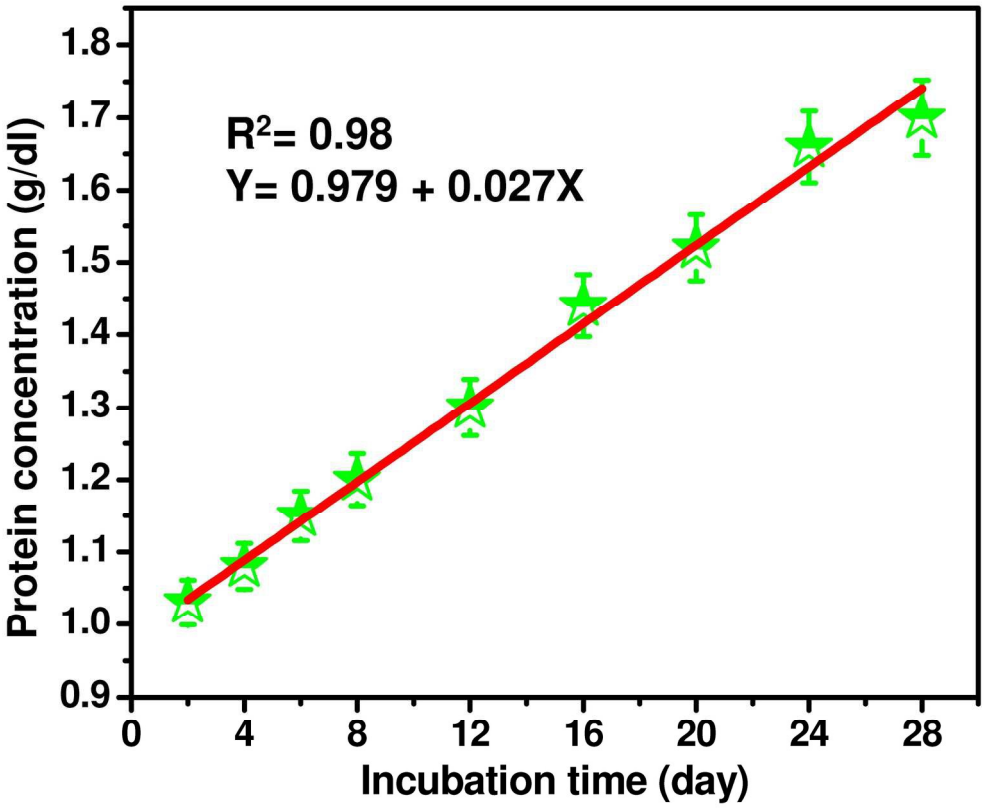

177x146mm (300 x 300 DPI)

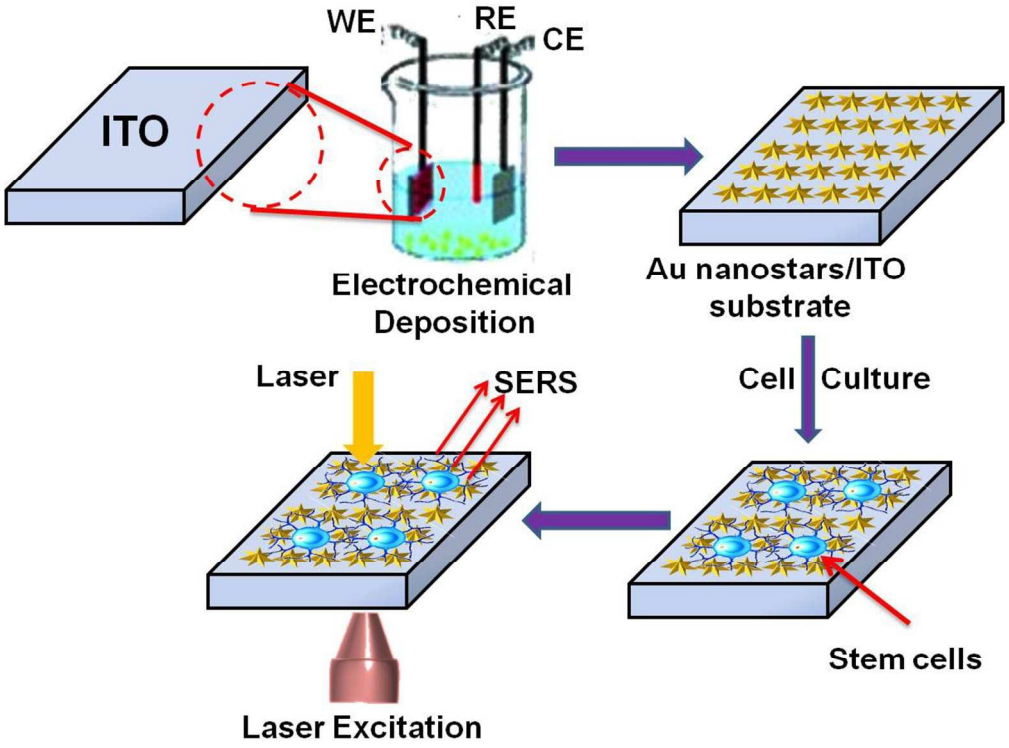

204x155mm (150 x 150 DPI)